CHAPTER 2

TOPOGRAPHICALLY-CONTROLLED THERMAL TIDES IN THE MARTIAN UPPER ATMOSPHERE

2.1 Abstract

Mars Global Surveyor accelerometer observations of the martian upper atmosphere have revealed large variations in density with longitude during northern hemisphere spring at altitudes of 130 – 160 km, all latitudes, and mid-afternoon local solar times (LSTs). This zonal structure is due to tides from the surface. The zonal structure is stable on timescales of weeks, decays with increasing altitude above 130 km, and is dominated by wave-3 (average amplitude 22% of mean density) and wave-2 (18%) harmonics. The phases of these harmonics are constant with both altitude and latitude, though their amplitudes change significantly with latitude. Near the South Pole, the phase of the wave-2 harmonic changes by 90° with a change of half a martian solar day while the wave-3 phase stays constant, suggesting diurnal and semidiurnal behaviour respectively. I use a simple application of classical tidal theory to identify the dominant tidal modes and obtain results consistent with those of General Circulation Models. My method is less rigorous, but simpler, than the General Circulation Models and hence complements them. Topography has a strong influence on the zonal structure.

2.2 Introduction

My objectives in Chapter 2 are to understand the nature of large variations in density with longitude observed in the martian upper atmosphere with the Mars Global Surveyor (MGS) accelerometer and to identify the underlying phenomena that cause them. I present a quantitative and detailed analysis of this zonal structure as a function of altitude, latitude, and local solar time (LST). I then use classical tidal theory to identify the dominant mechanisms causing the zonal structure, and finally outline a simple justification for topography having a strong influence on the zonal structure. I begin by quantifying the sol-to-sol (a sol is a martian solar day) variability, or weather, in the martian upper atmosphere and placing some constraints on its causes.

Accelerometer data from MGS's aerobraking phases revealed an unexpected phenomenon: the upper atmospheric density at fixed altitude, latitude, LST, and season varied by factors of 2 or more as a function of longitude (Keating et al., 1998). Corresponding atmospheric variabilities for the Earth, measured by the Satellite Electrostatic Triaxial Accelerometer at its reference altitude of 200 km altitude, are on the order of 10% (Forbes et al., 1999). For reference, typical atmospheric densities at 200 km altitude on Earth in Forbes et al. (1999) are $\sim$0.1 kg km^{-3} and typical atmospheric densities at 130 km altitude on Mars in this Chapter (Tables 2.2 and 2.3) are $\sim$1 kg km^{-3}. No such variations can be observed on Venus because its similar lengths of day and year do not allow all longitudes to have the same LST on a sub-annual timescale.

This zonal structure must originate in the lower atmosphere; it cannot be created *in situ*. There are no zonal inhomogeneities present in solar heating, which powers the dynamics of the martian atmosphere, or in the upper boundary of the atmosphere. There are many zonal inhomogeneities near the lower boundary of the atmosphere, including topography, surface thermal inertia, surface albedo, and lower atmosphere dust loading, which may influence this zonal structure. Since the

zonal structure must propagate through, and be affected by, the lower atmosphere, observations of the zonal structure in the upper atmosphere may reveal information about the properties of the lower atmosphere. This zonal structure is caused by atmospheric tides, which are global-scale atmospheric oscillations at periods which are subharmonics of a solar day (Forbes, 1995).

Keating et al. (1998) found that the zonal structure intensified during the build-up of a regional dust storm and, based on the constancy of its phasing, suggested that it was caused by topographically forced stationary waves. Several publications have presented theoretical simulations disagreeing with the stationary wave (disturbances which have no variation with time) hypothesis of Keating et al. (1998) for the zonal structure. Instead, nonmigrating tides, disturbances which vary with time but are not locked in phase with the Sun, are suggested (Keating et al., 1999; Keating et al., 2000; Forbes and Hagan, 2000; Joshi et al., 2000; Wilson, 2000a; Forbes et al., 2001). The restricted sampling in LST of the accelerometer data make these two types of disturbances impossible to distinguish observationally. Stationary waves are unlikely because they require an implausible vertical profile of zonal winds in the lower atmosphere if they are to be present in the upper atmosphere. All of these publications responding to Keating et al. (1998) predate the public release of the accelerometer dataset, hence they are based on the limited quantitative data presented in that paper and short conference abstracts discussing the complete accelerometer dataset (Keating et al., 1998; Keating et al., 1999; Keating et al., 2000). Here I present an analysis of the complete accelerometer dataset.

A previous publication has discussed the properties of the zonal structure, including its responses to changes in altitude, latitude, and LST, using the complete accelerometer dataset. Wilson (2002) observed that the zonal structure decreased in amplitude with increasing altitude and did not change in phase with changes in latitude. Wilson (2002) discussed the observation of Withers et al. (2000) that the zonal structure varied with half a sol changes in LST. Wilson (2002) did not present

quantitative results for how altitude or LST affected the zonal structure, nor did he quantify changes in the zonal structure on weekly timescales. Wilson (2002) only presented quantitative results for the strongest 2 components of the zonal structure, wave-2 and wave-3. In this chapter I present quantitative results for all these items, including the first four harmonic components of the zonal structure. Wilson (2002) compared his analysis of the MGS density data to General Circulation Model (GCM) predictions that accurately reproduced some aspects of the zonal structure, such as its amplitude and phase at 130 km and its changes with LST. He used them to identify the dominant tides causing the zonal structure (Wilson, 2002). Unlike Wilson (2002), I use my observations in conjunction with idealized classical tidal theory to identify the dominant tides. In this longer work I am able to go into more quantitative detail about the accelerometer dataset and choose a less rigorous, but simpler, theoretical approach to interpret my observations. I also outline a simple justification for topography, rather than any other surface physical property, being the strongest influence on the zonal structure.

The zonal structure and the tidal modes responsible for it have also been studied by other instruments onboard MGS, including the Thermal Emission Spectrometer (TES), the Mars Horizon Sensor Assembly, and the Radio Science experiment (Banfield et al., 2000; Banfield et al., 2003; Smith et al., 2001; Murphy et al., 2001; Bougher et al., 2001; Hinson et al., 2001; Tracadas et al., 2001).

The dynamics of the martian upper atmosphere are important for several reasons. Firstly, great cost savings are generated when a spacecraft aerobrakes into orbit around Mars, rather than using chemical propellant. Aerobraking is not possible without an understanding of the upper atmosphere, and improvements in this understanding yield great cost savings. Secondly, theoretical models of the upper atmospheres of Earth and Mars, regions which are very sensitive to changes in solar flux, share many key features. Understanding the upper atmosphere of Mars helps develop and verify these models, which can then be used, for example, to monitor changes in solar flux in Earth's upper atmosphere, an important measurement

for terrestrial climate change. Thirdly, as we shall see later in Section 2.6.1, the dynamics of the lower and upper atmosphere on Mars are strongly coupled, so by understanding the upper atmosphere we also learn about the lower atmosphere. The publicly available accelerometer dataset from the MGS spacecraft is a rich resource for studying the martian upper atmosphere (Keating et al., 2001a; Keating et al., 2001b). The results of this chapter contribute to a better understanding of the dynamics of the martian upper atmosphere.

The remainder of this chapter is divided into six parts. The first of these, Section 2.3, provides background information on the MGS accelerometer dataset.

In Section 2.4, Section 2.4.1 introduces the concept of sol-to-sol variability, or weather, *i. e.* changes between repeated density measurements at fixed altitude, latitude, LST, and season at intervals of one martian day, in the upper atmosphere. Section 2.4.2 presents my observations of the sol-to-sol variability and the implications each of them have for the nature of this variability. Finally, in Section 2.4.3, I sum up my constraints on the mechanism responsible for the sol-to-sol variability.

In Section 2.5, Section 2.5.1 introduces the zonal structure. Next, in Section 2.5.2, I examine how the amplitudes and phases of the harmonics making up the zonal structure change on timescales on the order of weeks. Section 2.5.3 continues this theme by examining how the amplitudes and phases of each harmonic in the zonal structure change as a function of altitude and see if this behaviour is affected by latitude. Section 2.5.4 follows by examining changes in the amplitudes and phases of each harmonic in the zonal structure as a function of latitude, discussing whether the cause of the zonal structure is planetary-scale or localized, and quantifying which harmonics are dominant. Finally, in Section 2.5.5, I compare the amplitudes and phases of harmonics in dayside and nightside zonal structures in polar regions.

In Section 2.6, Section 2.6.1 uses only the accelerometer data and classical tidal theory to make preliminary conclusions about which tides are causing the zonal

structure in the upper atmosphere. Section 2.6.2 discusses previous modelling and observational work on tides and the zonal structure and uses it to re-examine the preliminary conclusions of Section 2.6.1. Finally, in Section 2.6.3, I outline a simple justification for topography, rather than any other surface physical property, being the main underlying cause of the zonal structure.

Three short Sections complete this Chapter. Section 2.7 discusses the successful aerobraking of Mars Odyssey and the planned aerobraking of Mars Reconnaissance Orbiter. Section 2.8 discusses opportunities to extend and develop my studies of tides and zonal structure in the martian upper atmosphere. Finally, in Section 2.9, I state my main conclusions.

2.3 MGS Aerobraking

An aerobraking spacecraft, such as Mars Global Surveyor, passes through an atmosphere near the periapsis of its orbit and experiences an aerodynamic force which decreases the energy and semi-major axis of the spacecraft's orbit without the need for significant fuel consumption (French and Uphoff, 1979; Eldred, 1991). Aerobraking has previously been used by Atmospheric Explorer-C and its successors at Earth, the Pioneer Venus Orbiter at Venus, and Magellan at Venus (Marcos et al., 1977; Strangeway, 1993; Croom and Tolson, 1994; Lyons et al., 1995). Aerobraking permits *in situ* atmospheric studies not possible from a typical spacecraft orbit. The ill-fated Mars Observer, designed to use chemical propulsion for orbit insertion, launched on a $350M Titan III, whereas Mars Global Surveyor (MGS), reflying 5 of the 7 lost Mars Observer science instruments and designed to use aerobraking for orbit insertion, launched on a $50M Delta II (Lyons, 1996; Albee et al., 1998; Albee et al., 2001). This was the first use of aerobraking as an operational necessity in planetary exploration. Despite serious structural problems with the spacecraft, which restricted the maximum heating rate it could safely endure, and a severe dust storm raging in the atmosphere, MGS eventually reached its desired orbit and has

completed both its nominal and an extended mission (Tolson et al., 2000; Albee et al., 2001). Aerobraking would have been used by Mars Climate Orbiter, has been successfully used by Mars Odyssey, and is likely to be used by many future missions, including non-Mars missions.

MGS carried an Accelerometer Experiment (Keating et al., 1998; Keating et al., 2001a; Keating et al., 2001b). This accelerometer measured the aerodynamic forces on the spacecraft during an aerobraking pass. The accelerometer readings have been processed to generate a "profile" of atmospheric density along each flight path through the atmosphere (Keating et al., 1998; Cancro et al., 1998; Tolson et al., 1999; Tolson et al., 2000; Keating et al., 2001a; Keating et al., 2001b). This information was used by the spacecraft operations team in the hours immediately after the aerobraking pass to plan modifications to MGS's trajectory, changing the altitude of the next periapsis in steps of about 2 km by small expenditures of chemical propellant at apoapsis, to achieve the desired drag without exceeding heating rate thresholds, and guide it safely to the desired mapping orbit. MGS's orbit during aerobraking was near-polar, with an inclination of about 93°, and highly elliptical.

The changing characteristics of MGS's orbit during aerobraking were quite complicated and controlled the data coverage of the accelerometer. As such, they strongly influence the data analysis that I am able to do in Sections 2.4 and 2.5. I first discuss the orbital characteristics for the case when periapsis is away from the pole.

A typical aerobraking pass through the atmosphere lasted a few minutes and spanned several tens of degrees of latitude with only small changes in longitude or LST; unlike planetary entry probes or landers, the flight path of MGS through the atmosphere on each aerobraking pass is not vertical. On a typical aerobraking pass, latitude has a roughly quadratic dependence on altitude. The maximum altitude at which the accelerometer measured atmospheric density, set by the instrument sensitivity, was approximately 160 km. The minimum altitude at

which the accelerometer measured atmospheric density was that of periapsis, typically 110 km. Periapsis altitude was rarely outside 100–120 km. It often changed from one orbit to the next by a kilometre or so in response to the non-spherically symmetric gravitational field of Mars, in addition to any deliberate trajectory modifications. As aerobraking progressed, MGS's apoapsis altitude steadily decreased and the parabolic aerobraking pass through the atmosphere became flatter. A given altitude level was crossed twice on each aerobraking pass, once descending towards periapsis at one latitude and longitude, and once ascending after periapsis at another latitude and longitude. To distinguish between these two measurements at the same altitude and same orbit, I refer to the "inbound" and "outbound" legs of an aerobraking pass.

Since the near-polar orbit was close to sun-synchronous, periapsis LST changed only slowly between orbits. Periapsis longitude changed greatly between orbits as the planet rotated every 24.6 hours beneath MGS's orbit. The change in periapsis longitude per orbit, relative to 360°, was equal to the ratio of MGS's orbital period to the martian rotational period.

Periapsis latitude changed slowly but steadily between orbits. Due to the oblateness of Mars, the orbit precessed around in its orbital plane (Murray and Dermott, 1999). This caused periapsis latitude to change. The entire parabolic flight path also shifted in latitude as the orbit precessed. Due to this precession, I can analyse densities at a range of altitudes, but fixed latitudes, from the non-vertical aerobraking passes (Section 2.5.3) and analyse densities at a range of latitudes, but fixed altitudes (Section 2.5.4). To summarize, MGS had a slowly flattening, parabolic flight path through the atmosphere, travelled in either a north or south direction with small changes in LST and longitude during a pass, with large changes in longitude due to the planet's rotation, small changes in LST, and steady changes in latitude between periapses.

The picture is more complicated when periapsis is in the polar regions. This is discussed in Section 2.5.5.

Aerobraking took place in two Phases, 1 and 2, separated by a hiatus containing the Science Phasing Orbits (Albee et al., 1998; Albee et al., 2001). Phase 1 included orbits 1 – 201 from mid-September, 1997, to late March, 1998, and Phase 2 included orbits 574 – 1283 from mid-September, 1998, to early February, 1999. This covers a range of martian seasons. L_S, martian heliocentric longitude, is 0° at the northern spring equinox, 90° at the northern summer solstice, 180° at the northern autumn equinox, and 270° at the northern winter solstice. At the beginning of Phase 1, $L_S = 180°$, periapsis occurred at 30°N and 18 hrs LST, then moved northwards and earlier in the day to reach 60°N and 11 hrs LST at the end of Phase 1, $L_S = 300°$. One "hour" of LST is equal to 1/24th of a sol, not 60 minutes of elapsed time. MGS flew from north to south through the atmosphere on each aerobraking pass during Phase 1. At the beginning of Phase 2, during the next martian year at $L_S = 30°$, periapsis occurred at 60°N and 17 hrs LST, then moved southwards and earlier in the day to cross 80°S at 15 hrs LST. At the beginning of Phase 2, MGS flew from south to north through the atmosphere on each aerobraking pass. Periapsis then reached its farthest south ($\sim$ 87°S) near the south pole, crossed the terminator by drifting through nighttime LSTs, and reached 60°S and 02 hrs LST by the end of Phase 2, $L_S = 90°$. At the end of Phase 2, MGS flew from north to south through the atmosphere on each aerobraking pass. When periapsis was near the south pole, each aerobraking pass's profile of atmospheric density spanned a large range of LST. The behaviour of periapsis during aerobraking is summarized in Figure 2.1.

In this chapter, I discuss two broad subsets of the accelerometer data, both from Phase 2 of aerobraking. The Phase 1 data are complicated by significant changes in both periapsis latitude and LST between each orbit and by the presence of a regional dust storm, so I leave them for future work. Some work on the Phase 1 data has previously been published (Keating et al., 1998; Bougher et al., 1999). The two subsets of data from Phase 2 are: (1) the southward progression from 60°N to 60°S at almost fixed L_S and LST at the beginning of Phase 2 and (2) the crossing of the south pole from 60°S back to 60°S at almost fixed L_S and two

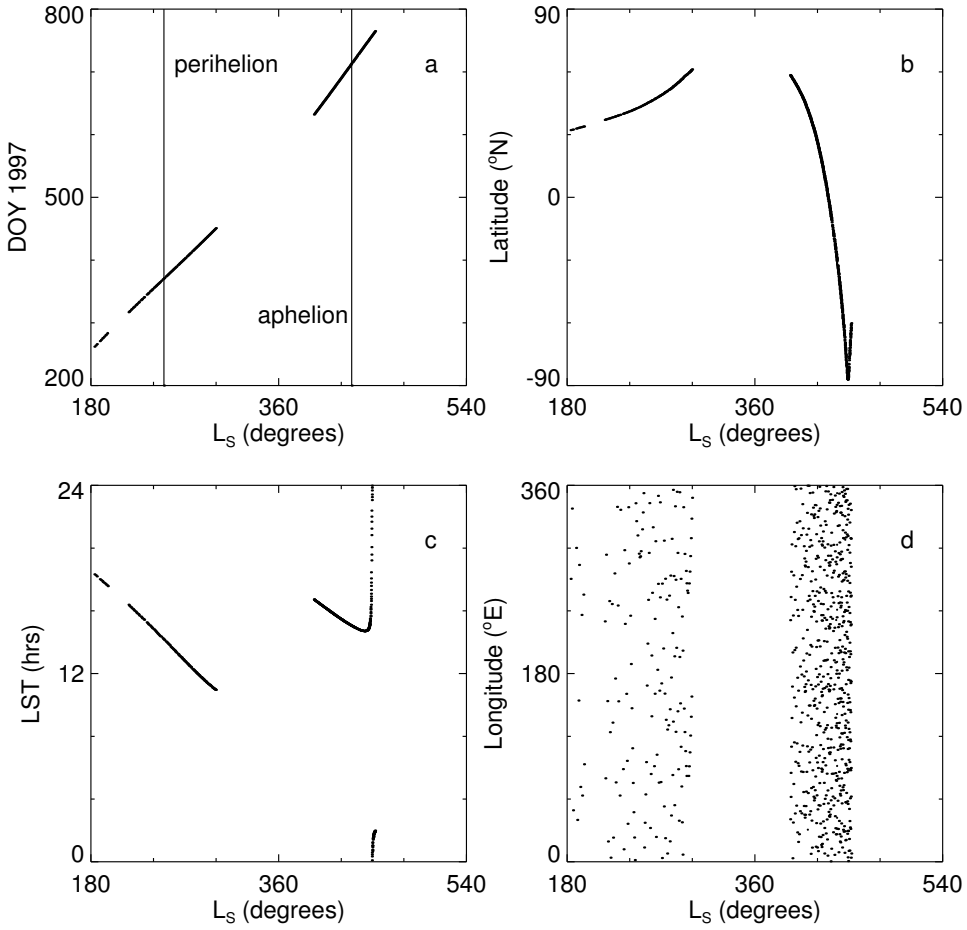

Figure 2.1: Parameters of periapsis during aerobraking: (a) periapsis date in days since Jan 1, 1997 (DOY 1997), (b) periapsis latitude, (c) periapsis LST, and (d) periapsis longitude, all plotted against heliocentric longitude, L_S. Phase 1 of aerobraking occured before $L_S = 360°$ and Phase 2 afterwards. The change from daytime to nighttime LSTs as periapsis reached its furthest south can be seen at $L_S \sim 450°$. The L_S of perihelion and aphelion are marked on panel (a) for reference.

different LSTs, half a sol apart, at the end of Phase 2. I name these two subsets of data the "Daytime Precession" (subset 1) and the "Polar Crossing" (subset 2). The boundary between these two subsets is defined as when a specified point on the aerobraking pass crosses the 60°S boundary on the dayside part of Phase 2. When discussing, for example, data at 130 km altitude from the inbound leg of aerobraking passes, all aerobraking passes in which the latitude at 130 km on the inbound leg is south of 60°S are classified in the Polar Crossing part of Phase 2. For data at different altitudes, or from the other leg of the aerobraking pass, a slightly different group of aerobraking passes forms the Polar Crossing part of Phase 2. As a rough guide, the first periapsis latitude southward of 60°S occurred on orbit 1095.

Data from the Accelerometer Experiment is archived in the Planetary Data System (PDS) (Keating et al., 2001a). This dataset contains 800 upper atmospheric density profiles. The only previous three are those of the Pathfinder and two Viking landers (Magalhães et al., 1999; Seiff and Kirk, 1977a). Also archived are data extracted from 768 of these profiles at 130, 140, 150, and 160 km altitude on both the inbound and outbound legs of each aerobraking pass (Keating et al., 2001b). The constant altitude data were used for this work. Many orbits between 911 and 961, during the Daytime Precession part of Phase 2 of Aerobraking, do not have density data due to spacecraft computer problems. Data and results affected by this are highlighted in the text.

Previous work on this dataset includes Angelats i Coll et al. (2001), Bougher et al. (1997), Bougher and Keating (1999), Bougher et al. (1999), Bougher et al. (2000), Bougher et al. (2000), Bougher et al. (2001), Bougher et al. (2001), Forbes (1999), Forbes and Hagan (2000), Joshi et al. (2000), Keating et al. (1998), Keating et al. (1999), Keating et al. (1999), Keating et al. (2000), Keating et al. (2001), Tolson et al. (1999), Tolson et al. (2000), Wilson (2000b), Wilson (2002), Withers et al. (1999), Withers et al. (2000), Withers et al. (2001a), Withers et al. (2001b), Withers et al. (2002b), Withers et al. (2002a), and Withers et al. (2002c). There have been few peer-reviewed publications analysing this dataset, so there is

not a comprehensive bibliography anywhere in the literature of existing work on this dataset.

2.4 Sol-to-Sol Variability

2.4.1 Introduction to Sol-to-Sol Variability

In this section I quantify sol-to-sol variability in the atmosphere to test whether I can meaningfully compare density measurements made at different longitudes on different days as if they were made simultaneously. Such comparisons are important in the remainder of this chapter.

During aerobraking, the orbital period of MGS decreased from over 30 hours to less than two hours. Whenever the orbital period was a submultiple of Mars's 24.6 hour rotational period, repeated density measurements were made along essentially the same flight paths, that is longitude/altitude/latitude, at one sol intervals. When the rotational period is n times the orbital period, then I say that MGS is in the n:1 resonance. Such a "resonance" typically lasted for several sols as the orbital period decreased through the resonance condition. In the 1:1 resonance, an aerobraking pass traces the same altitude/latitude/longitude path as the one before it. In the 2:1 resonance, there are two different altitude/latitude/longitude paths 180° apart in longitude traced through the atmosphere on each aerobraking pass, each traced by every second one. In the n:1 resonance, paths are $360°/n$ apart, each traced by every nth aerobraking pass. If the outbound legs at, say, 130 km are considered, and the latitudes and longitudes of each orbit in the n:1 resonance are plotted, then they form n clusters separated by $360°/n$ of longitude. I study the different density measurements taken in these very restricted altitude/latitude/longitude clusters during various resonances. If the atmosphere does not change from one sol to the next, then all the measurements in a given cluster should be the same. My measure of the sol-to-sol variability is the standard deviation of the density measurements

in a cluster, expressed as a percentage of the mean of the density measurements in that cluster. For example, the number "50" implies a standard deviation equal to half of the mean.

This analysis is important for determining how much of the difference between density measurements at different longitudes and sols is due to zonal structure and how much is due to temporal variations. The sol-to-sol variability is an important parameter in mission planning and operations involving aerobraking, such as the current planning for Mars Reconnaissance Orbiter.

Orbits were assigned to the n:1 resonance if their periods were within 3% of the appropriate submultiple of the martian sidereal day. With this criterion, the latitudes and longitudes at, say, 130 km on the inbound leg of each orbit in the resonance formed well-defined clusters (typically 10° wide in longitude and somewhat narrowerer in latitude) with enough orbits in each cluster to measure a meaningful atmospheric sol-to-sol variability.

As an example, I show in Figure 2.2 the four trajectories and density profiles whose periapsis longitudes were within ±5° of 135°E during the 7:1 resonance. These are periapses 963, 970, 977, and 984. Periapsis latitude progressed southward as periapsis number increased, so periapsis 963 is the northernmost aerobraking pass in Figure 2.2. Three density profiles are very similar, but the periapsis 977 profile is significantly different.

In summary, occasional repeat measurements at one sol intervals along nearly identical flight paths can constrain the sol-to-sol variability in the martian upper atmosphere at fixed longitude, altitude, latitude, and LST.

2.4.2 Observations of Sol-to-Sol Variability

Figure 2.3 shows the sol-to-sol variability for the 3:1 to 8:1 resonances. These resonances occurred during the Daytime Precession part of Phase 2. Crosses

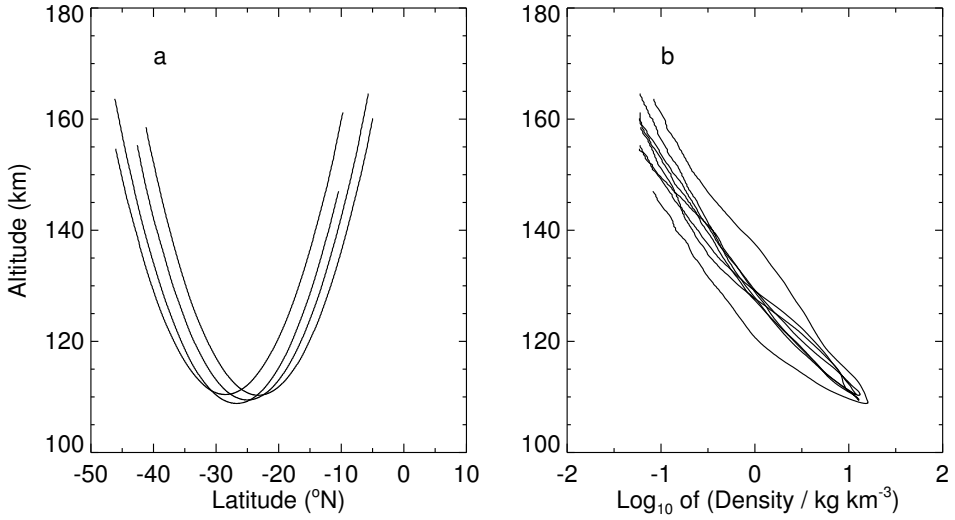

Figure 2.2: Trajectories (a) and density profiles (b) for periapses within $\pm 5°$ of 135°E during the 7:1 resonance. From the north, periapsis numbers are 963, 970, 977, and 984. Periapsis 977's density profile is significantly different from the others.

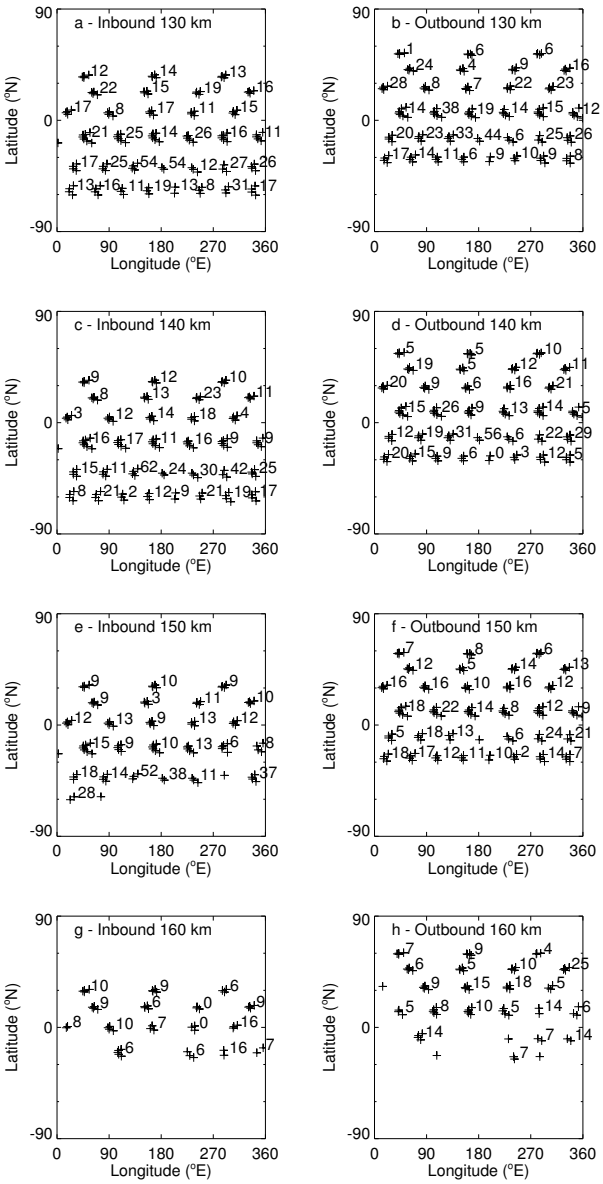

Figure 2.3: Latitudes and longitudes of clustered density measurements made at 130, 140, 150, and 160 km altitude on inbound and outbound legs during the 3:1 — 8:1 resonances, plotted as crosses. The number adjacent to each cluster of crosses is the sol-to-sol variability for that cluster.

mark the latitude and longitude of each density measurement at a certain altitude whose orbital period satisfies my resonance criterion. Fewer crosses are plotted at higher altitudes because many orbits do not have good density measurements at the higher altitudes. This is especially common in the southern (winter) hemisphere, where observed densities were lower than at corresponding northern (summer) latitudes. Each row of crosses on a panel in Figure 2.3 corresponds to a different resonance. The n:1 resonance contains n clusters at equally spaced longitudes. By counting the numbers of clusters at a given latitude in a panel of Figure 2.3, n for that resonance can be found. This does not work so well at the higher altitudes where nothing is plotted for some clusters, because none of the orbits which belong to those clusters have valid density measurements at those altitudes. On panel (a), data in the northernmost three clusters were collected over a few days during the 3:1 resonance. During those same few days of the 3:1 resonance, data in the northernmost three clusters on each panel were collected. A couple of weeks later, data in the second row of four clusters were collected for each panel. On each panel, the same orbits contribute to, say, the northernmost and easternmost cluster. The n:1 resonance at any altitude is farther north on outbound than inbound. The latitude of the outbound (inbound) n:1 resonance at a given altitude is further north (south) than at any lower altitude. The numbers adjacent to each cluster are my measure of the sol-to-sol variability in that cluster. Table 2.1 gives the periapsis latitude, periapsis LST, L_S, and beginning and ending periapsis numbers for each resonance. Periapsis number n was the nth periapsis during the MGS mission.

1σ measurement errors in the individual density measurements are about 3% or less over 130 – 150 km, increasing to 5% at 160 km (Keating et al., 2001b). These are negligible compared to the sol-to-sol variability at 130 – 150 km altitude. At 160 km, the 5% measurement error is smaller than the average sol-to-sol variability of 8 – 10%, suggesting that I am actually observing sol-to-sol variability and not merely errors in individual measurements. The sol-to-sol variability decreases with increasing altitude. It averages 15 – 20% at 130 km and 8 – 10% at 160 km. This is consistent with dissipative processes operating on upwardly propagating

Resonance	L_S (degrees)	Latitude (°N)	LST (hrs)	Beginning Periapsis	Ending Periapsis
3:1	48	45	16	645	656
4:1	57	32	16	710	725
5:1	64	16	15	784	803
6:1	71	−4	15	864	901
7:1	78	−28	15	963	989
8:1	82	−45	15	1030	1057

Table 2.1: L_S, periapsis latitude, periapsis LST, and beginning and ending periapsis number for the 3:1 – 8:1 resonances.

disturbances (Zurek et al., 1992; Forbes et al., 2001).

At a given altitude, latitude, LST, and season, the sol-to-sol variability is not constant from one longitude region to the next. A few hours separates measurements at one longitude region on a given sol from measurements at the neighbouring longitude region on the same sol. The sol-to-sol variability often changes significantly over longitude intervals of only 60°. Either the solar forcing is varying significantly on timescales of a few hours or the sol-to-sol variability is in some way affected by the local properties of the planetary surface far below.

There is no obvious difference between sol-to-sol variabilities in the tropics and in the extratropics, so the sol-to-sol variability cannot be caused by a mechanism that is filtered out beyond certain latitudes, such as inertio-gravity waves with periods of one sol or longer (Houghton, 2002). At the highest northern, but not southern, latitudes the sol-to-sol variability is significantly lower than is typical. This difference between the inbound and outbound legs of the 3:1 resonance could be due to effects from the planetary surface or differences in the atmospheric dynamics between the near-winter polar regions and elsewhere; it can't be due solely to solar flux variations.

Compare, for example, the inbound and outbound 8:1 resonances at 130 km. The inbound example, at 60°S, has its lowest value of sol-to-sol variability at 250°E and its highest at 290°E, yet the outbound example, at 30°S and including the same aerobraking passes, has its lowest value at 150°E and its highest at 20°E. This is one example, and others can be seen in Figure 2.3, of changes in the sol-to-sol variability over meridional length scales of several tens of degrees. This is in contrast to the zonal structure, discussed from Section 2.5 onwards, which has no significant changes over similar meridional length scales.

Compare, for example, the outbound 7:1 resonances at 130 and 140 km. The lower example has its lowest value of sol-to-sol variability at 220°E and its highest at 180°E. So has the other example, 10 km higher up. This is one example, and others

can be seen in Figure 2.3, of sol-to-sol variabilities at one altitude level being related to sol-to-sol variabilities at the neighbouring altitude level. This implies that the vertical length scale for changes in the sol-to-sol variability at one longitude relative to another is greater than 10 km.

The sol-to-sol variability at fixed altitude and latitude is not constant from one observation using inbound data to another observation, a few weeks later at the same altitude and latitude, using outbound data during a different resonance. Neither its pattern of high and low values as a function of longitude nor its zonally-averaged value is constant. For example, the inbound leg of the 6:1 resonance and the outbound leg of the later 7:1 resonance both occurred around 10° – 20°S, yet the zonal mean of the sol-to-sol variabilities is significantly higher for the outbound leg of the 7:1 resonance compared to the inbound leg of the 6:1 resonance. The inbound leg of the 6:1 resonance has low sol-to-sol variabilities around 220°E flanked by higher variabilities, yet the outbound leg of the 7:1 resonances has high variabilities around 220°E flanked by lower variabilities. This suggests that the time scale for change in the sol-to-sol variability is less than several weeks, *i. e.* short on seasonal timescales, and that the sol-to-sol variability is not simply a function of properties of the underlying surface.

Sol-to-sol variability as a function of longitude is not correlated with the elevation of the topography below, so the sol-to-sol variability is not significantly affected by a few km difference in the distance propagated through the lower atmosphere.

Later in the mission, during the Polar Crossing part of Phase 2, inbound and outbound legs of an aerobraking pass spanned similar latitudes on opposite sides of the pole. During the 11:1 resonance, inbound measurements at 130 km were made at $70° - 80°$S and LST = 01 hours and outbound measurements at the same altitude were made a few minutes later at $60° - 70°$S and LST = 15 hours. Data at higher altitudes are not available. In this case, I extended my resonance criterion from periods within 3% of resonance to 4% to have enough measurements

in most clusters. Figure 2.4 shows significant LST dependence in relative sol-to-sol variability as function of longitude, though both dayside and nightside measurements have average sol-to-sol variabilities in the typical 15 – 20% range for 130 km altitude.

High sol-to-sol variabilities do not coincide with high densities in the zonal structure, which can be seen in Section 2.5.4. The sol-to-sol variability is not correlated with the zonal structure, so they have different causes.

In summary, the mechanism(s) responsible for the sol-to-sol variability has a vertical length scale greater than 10 km, a meridional length scale less than several tens of degrees, a zonal length scale less than 60 degrees, and a timescale shorter than several weeks. The sol-to-sol variability weakens with increasing altitude, is affected by changes in LST, and is not restricted in latitude. As discussed later in Sections 2.5.2 and 2.5.4, the mechanism responsible for the zonal structure has different properties, specifically longer time and meridional scales.

2.4.3 Discussion of Sol-to-Sol Variability

In this section I discuss the implications of the previous section and other work for the cause of the sol-to-sol variability. I also make predictions about the sol-to-sol variability to be compared against future observations.

Sol-to-sol variations in density due solely to short-term solar flux variations have been observed in data from Phase 1 of aerobraking. Keating et al. (1998) observed a 50% increase in density at 160 km altitude at both 32°N and 57°N near orbit 90, with no significant change in density at 130 km altitude, at the same time as an increase in the extreme ultra-violet solar flux incident upon the martian atmosphere. The decrease in sol-to-sol variability with increasing altitude in this Section, in contrast to the increase in sol-to-sol variability with increasing altitude in the Keating et al. (1998) example, suggests a mechanism beyond just short-term solar flux variations.

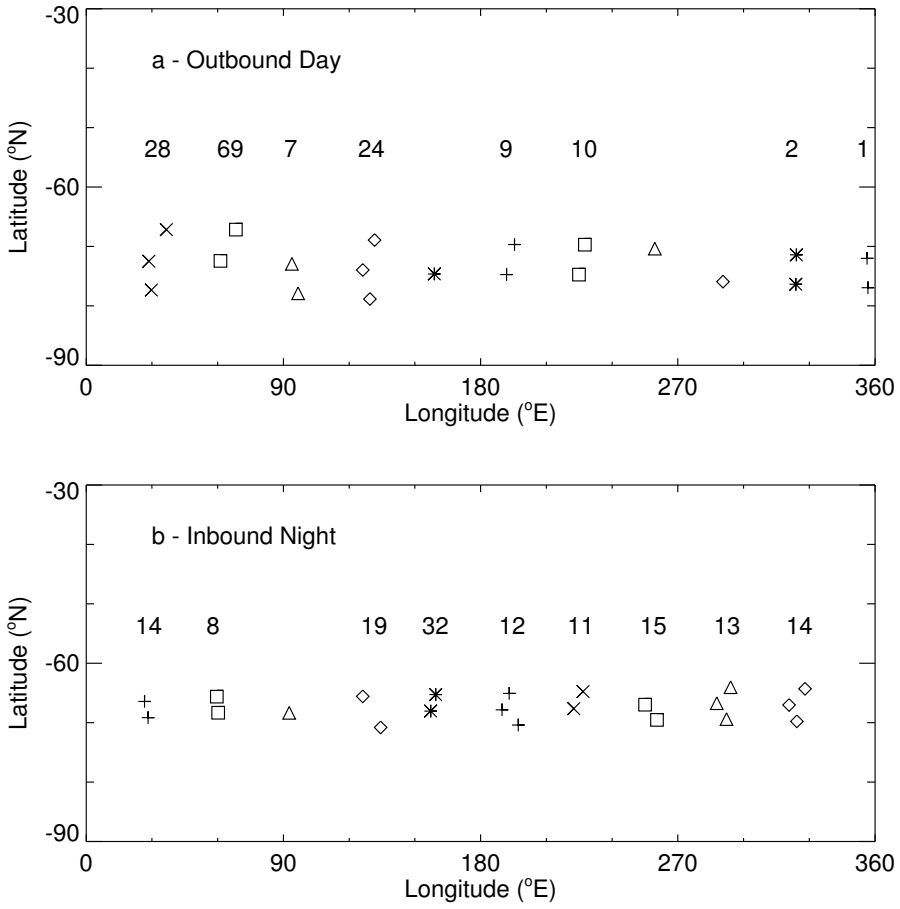

Figure 2.4: Locations of repeat samplings at 130 km during the 11:1 resonance and sol-to-sol variability in each cluster, as discussed in Section 2.4.2. To aid identification of the clusters, all measurements in a given cluster have the same symbol and neighbouring clusters have different symbols.

Several observations from the MGS Radio Science experiment may shed light on this subject (Tyler et al., 2001). Tracadas et al. (2001) studied changes in the orbit of MGS during the Science Phasing Orbits and concluded that at 180 km altitude and latitudes north of 60°N the orbit-to-orbit variability of atmospheric density at $L_S = 300° - 360°$ and LST= 13 hours was 50 – 70%, whereas at $L_S = 0° - 30°$ and LST= 07 hours it was 10 – 20%.

Tracadas et al. (2001) also concluded that no zonal structure was present. Their orbit-to-orbit variability may not be due solely to sol-to-sol variability, since it may be affected by zonal variability that does not have the well-behaved form of the zonal structure. Since zonal variability should asymptote to zero at high altitudes I shall assume that this orbit-to-orbit variability is purely sol-to-sol variability. Their 10 – 20% variability at 180 km altitude near the beginning of the Daytime Precession part of Phase 2 is similar in scale to my 8 – 10% variability at 160 km during the Daytime Precession part of Phase 2. Either the sol-to-sol variability in the upper atmosphere was greater during their observations than mine or the sol-to-sol variability does not decrease monotonically with increasing altitude above the 130 – 160 km region.

Hinson et al. (2001) analysed temperature profiles as a function of pressure from 0 – 50 km altitude at $L_S = 74° - 77°$, 04 hours LST, and latitude = 65°N. They found sol-to-sol variability of less than 2% but significant variability with longitude. These measurements were made between the 6:1 and 7:1 resonances. My measurements, at the earlier L_S of 48° during the 3:1 resonance, of the sol-to-sol variability in the upper atmosphere at $55 - 60$°N are the closest to these in latitude. These northernmost measurements have the lowest sol-to-sol variability of any in Figure 2.3. These observations suggest that sol-to-sol variability in the lower and upper atmospheres is low at far northern latitudes during this season. Equivalent southern latitudes have sol-to-sol variability in the upper atmosphere that is typical of Figure 2.3.

Current GCMs are climate, not weather, models, so they cannot directly

simulate the sol-to-sol variability (Murphy et al., 1995; Forget et al., 1999; Bougher et al., 2000; Wilson, 2000a). However, they could be used to place additional constraints on the possible mechanisms causing the sol-to-sol variability. For example, regions that launch strong gravity waves and also permit them to propagate to the upper atmosphere may be correlated with those that have high sol-to-sol variabilities. However, the current focus of my work is on understanding the zonal structure, so I do not address these issues further in this chapter.

The sol-to-sol variability at the highest northern latitudes is consistently below average. There is a wide variation in sol-to-sol variability over changes in longitude of less than 60°. Neither of these observations can be explained by solar flux variations alone. High sol-to-sol variability might be explained by gravity waves preferentially propagating upwards from certain places when atmospheric conditions are favorable. This is just one possible mechanism, but I do not investigate this any further in this chapter.

Preflight estimates of the orbit-to-orbit variability, which includes effects from both sol-to-sol and zonal variabilities, of 35% were realistic (Stewart, 1987; Tolson et al., 1999). The sol-to-sol variability of 15 – 20% accounts for part of this, with variations in density with longitude accounting for the rest. For comparison, the Earth's day-to-day variability at 200 km altitude can be on the order of 50% during magnetic storms, Venus's nighttime density at 150 km can vary by factors of two over 24 hours, yet its daytime density varies by less than 10% over the same period (Forbes et al., 1996; Keating et al., 1979; Lyons, 1999).

An estimate of likely orbit-to-orbit variability is a critical part of JPL's ongoing preperation for the aerobraking of Mars Reconnaissance Orbiter in 2005. What predictions can I make for the sol-to-sol variability that might be experienced by this and other future missions? If the MGS Phase 2 Aerobraking period is representative, then I predict sol-to-sol variabilities of 15 – 20% at 130 km, decreasing with increasing altitude. Periods of significantly above-average and below-average sol-to-sol variability should be expected. I am unable to make any predictions for

how the sol-to-sol variability may vary with LST, longitude, and latitude, I have no evidence to suggest that the sol-to-sol variabilities remain the same from one season to the next. The martian climate has enough inter-annual variability that the characteristics of the sol-to-sol variability could even change significantly from year to year.

New measurements will, of course, be useful in understanding this phenomenon, but they will be most useful if they are designed to allow a thorough sampling of one possible influencing factor whilst keeping the others fixed. Without this level of experimental control, it will be difficult to disentangle the various effects of latitude, longitude, LST, solar flux variations, and so on.

To answer the question posed at the beginning of this Section, it is reasonable to compare density measurements made at different longitudes several days apart as long as differences in density smaller than or similar to the sol-to-sol variability of 15 – 20% are not automatically attributed to zonal variations.

In summary, the sol-to-sol variability appears to require a mechanism beyond just solar flux variations, such as gravity waves, is an important constraint on aerobraking planning and operations, and is very different on Mars from that on Venus or Earth.

2.5 Observations of the Zonal Structure

2.5.1 Introduction to the Zonal Structure

I now move on from studying density measurements at fixed longitude, altitude, latitude, and LST to studying density measurements at varying longitudes and fixed altitude, latitude, and LST. Keating et al. (1998) discovered that large, regular variations in density with longitude exist in the martian upper atmosphere. Similar variations on Earth are significantly smaller (Forbes et al., 1999). Now that I have

constrained how much sol-to-sol variability exists, I can examine this zonal structure in density. In this section I discuss my technique for fitting a model to the observed zonal structures.

When MGS's orbital period is not in resonance with the rotational period of Mars, reasonably complete longitudinal coverage is obtained from a small set of consecutive orbits due to the changes in periapsis longitude between each orbit. As periapsis latitude precesses between each orbit, there is a finite range of periapsis latitude in this subset of the data. The same reasoning applies to building up a picture of the zonal structure at a fixed altitude, say 130 km on the outbound legs of aerobraking passes — reasonably complete longitudinal coverage can be obtained over a narrow range in measurement latitude. Figure 2.5 shows outbound densities at 130 km altitude between 10°S and 20°S from the Daytime Precession part of Phase 2 of aerobraking. This illustrates the zonal structure. LST (14.7 – 14.8 hrs) and L_S (77–80°) are effectively constant for these measurements. Periapsis precessed southward between 10°S and 20°S with large changes in periapsis longitude between each periapsis. The longitudinal sampling is not built up in a regular pattern (*e. g.* from east to west) and measurements that appear to sample the same longitude repeatedly are not from consecutive orbits. During this period, MGS travelled from south to north on each aerobraking pass with its periapsis between 24°S and 33°S at altitudes of between 108 and 112 km. These data were taken during the 7:1 resonance, a period of significant sol-to-sol variability as can be seen in Figure 2.3. Despite the variability in measurements at a given longitude, *e. g.* 90°E, it is immediately apparent that regular variations in density with longitude exist in the upper atmosphere of Mars. Density varies by a factor of two over 90° of longitude, greater than the sol-to-sol variability.

Measurement uncertainties are not shown in Figure 2.5. As discussed in Section 2.4, they do not become comparable to the sol-to-sol variabilities until altitudes greater than 150 km. I use a least-squares fit to a wave-4 model to characterize the zonal structure. This model contains a constant density term, an amplitude

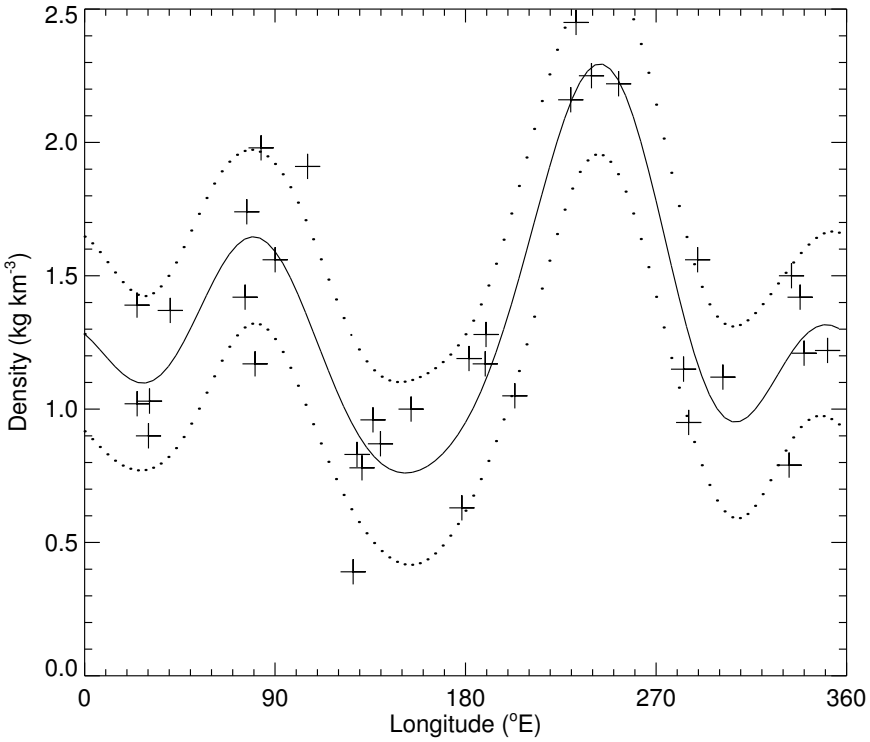

Figure 2.5: All outbound density measurements at 130 km altitude between 10°S and 20°S from the Daytime Precession part of Phase 2, crosses, wave-4 harmonic model fit to the data, solid line, and 1σ uncertainties about the fit, dotted lines. The data were collected over about a week, all at an LST of 15 hrs. Measurement uncertainties (not shown) are much smaller than the range in multiple measurements at any longitude. Zonal structure with large peaks in density at 90°E and 250°E can be seen.

and phase for a sinusoid with one cycle per 360° of longitude, which I label as the wave-1 harmonic, and higher harmonics up to and including wave-4. It has 9 free parameters. Measurement uncertainties are not used to constrain the fit. A wave-4 model was chosen because wave-3 models had significantly worse fits to the data in the Daytime Precession part of Phase 2 of aerobraking and wave-5 models did not have significantly better fits. The details of the model and the fitting procedure are discussed in Appendix A. The error envelope plotted on Figure 2.5 shows a 1σ uncertainty on what a single new observation at a given longitude might be. I define the phase of a given harmonic as the longitude of its first peak east of 0°. The phase of the wave-n harmonic must lie between 0° and 360°E/n. I generally normalized the zonally-varying terms in each wavefit by their constant density term. This facilitates a comparison of the strength of the zonal structure between different seasons or altitudes.

Throughout this chapter, I only attempted model fits to more than 15 data points and only accepted the fit as good if there was a 90% probability that not all model parameters beyond the constant density term should be zero (Neter and Wasserman, 1974). Bad fits generally occurred in regions where there were significantly fewer data points than usual, which might be due either to data dropouts or to a high rate of periapsis precession through a given latitude range. If fewer than 16 data points were available, then I did not attempt a fit.

In summary, large zonal structures in density are present in the martian upper atmosphere, even during periods of high sol-to-sol variability, and I characterize them with a wave-4 harmonic fit.

2.5.2 Changes in Zonal Structure on Weekly Timescales

As periapsis latitude precessed between orbits, the entire parabolic flight path through the atmosphere shifted with it. This changed the latitude at which MGS passed through, say, 130 km on its outbound leg.

If, as during the Daytime Precession part of Phase 2 of aerobraking, periapsis precesses southward as MGS travels from south to north during each aerobraking pass, then first the 130 km measurement on the inbound leg, and later the same measurement on the outbound leg, occur at a given latitude.

This gives me two separate opportunities, inbound and outbound, a few weeks apart, to study the atmospheric density at a given latitude, altitude, season, and LST. Season and LST are changing much more slowly than periapsis latitude is precessing. Since periapsis longitude (which is the same as the longitude of the rest of the aerobraking pass away from the polar regions) is continuing to change from one orbit to the next, a picture of the zonal structure at a given latitude range and altitude can be built up on these two separate occasions. In this section I examine how the amplitudes and phases of the harmonics making up the zonal structure change between these two samplings and discuss whether data from the two samplings should be combined or kept separate.

Figure 2.5 shows *outbound* densities at 130 km altitude between 10°S and 20°S from the Daytime Precession part of Phase 2 of aerobraking. Figure 2.6 shows *inbound* densities at 130 km altitude between 10°S and 20°S from the Daytime Precession part of Phase 2 of aerobraking. The inbound measurements, taken during the 6:1 resonance, were made about two weeks prior to the outbound measurements. The data in each figure were collected over a period of one week. Changes in the zonal structure in this example are minor. Table 2.2 shows how the amplitudes and phases of the various harmonics change. Only the wave 1 amplitude and wave 2 phase have changed in a statistically significant sense. Recall that the maximum value of the wave-n phase is $360°\mathrm{E}/n$.

Figure 2.7 shows the interval between repeated density measurements at 130 km altitude as a function of latitude for the Daytime Precession part of Phase 2. Figure 2.1 shows that changes in LST and L_S are small on these timescales. This allows me to characterize the zonal structure at a given altitude, latitude, LST, and L_S twice — with an interval on the order of several weeks between the

Parameters	Inbound	Outbound
Constant Amplitude (kg km^{-3})	1.324 ± 0.042	1.337 ± 0.051
Normalized Wave 1 Amplitude	0.054 ± 0.045	0.165 ± 0.055
Normalized Wave 2 Amplitude	0.249 ± 0.058	0.345 ± 0.055
Normalized Wave 3 Amplitude	0.204 ± 0.059	0.177 ± 0.071
Normalized Wave 4 Amplitude	0.105 ± 0.058	0.109 ± 0.065
Wave 1 Phase (degrees)	298.7 ± 47.7	260.5 ± 18.3
Wave 2 Phase (degrees)	80.4 ± 6.4	64.1 ± 4.5
Wave 3 Phase (degrees)	103.0 ± 5.1	109.6 ± 7.2
Wave 4 Phase (degrees)	81.5 ± 7.7	74.0 ± 9.7

Table 2.2: Model fit parameters for measurements made between 10–20°S during the Daytime Precession part of Phase 2. Uncertainties are 1σ.

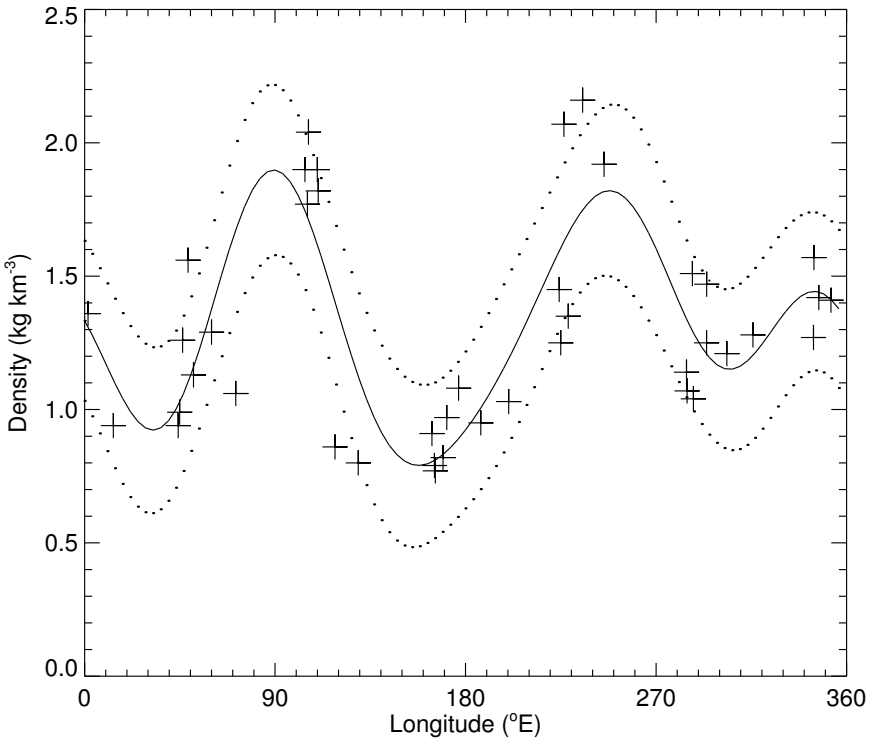

Figure 2.6: As Figure 2.5, but showing inbound data collected in the same latitude range a couple of weeks earlier. The data were also collected over about a week, all at an LST of 15 hrs. The amplitudes of the two large peaks have changed somewhat, but their phases have not. The zonal structure is stable on timescales of a couple of weeks.

two characterizations.

This leaves me with two options: I may either combine inbound and outbound measurements to characterize a given altitude, latitude, LST, and L_S once only or treat these two halves separately. Combining measurements gives more data points but introduces the issue of having half the data collected over a week, a week of no data, then a week of collecting the last half of the data. Wilson (2002) notes that the meridional variation of zonal mean density is the same for inbound and outbound, further notes that there is little difference between the zonal structure observed in inbound and outbound data, and then uses inbound and outbound data together. Until I have carefully investigated the statistical similarity of the inbound and outbound wavefits at a given altitude, latitude, LST, and L_S I keep inbound and outbound measurements separate. Each data collection period is thus continuous.

In summary, the zonal structure during the Daytime Precession part of Phase 2 of aerobraking is stable on timescales of a couple of weeks. This is in contrast to the sol-to-sol variability, which has a shorter timescale.

2.5.3 Changes in Zonal Structure With Altitude

In this section I characterize how the amplitudes and phases of each harmonic in the zonal structure change as a function of altitude and see if this behaviour is affected by latitude.

Density measurements are made at every altitude on each leg of an aerobraking pass. Densities at one altitude can be compared with those at another altitude from the same leg. However, since the two densities are also measured at different latitudes, the comparison does not isolate changes due to altitude alone. Due to the precession of periapsis and with it the entire parabolic flight path through the atmosphere, a density measurement at one altitude and latitude on the outbound leg of an aerobraking pass can be compared to another density measurement

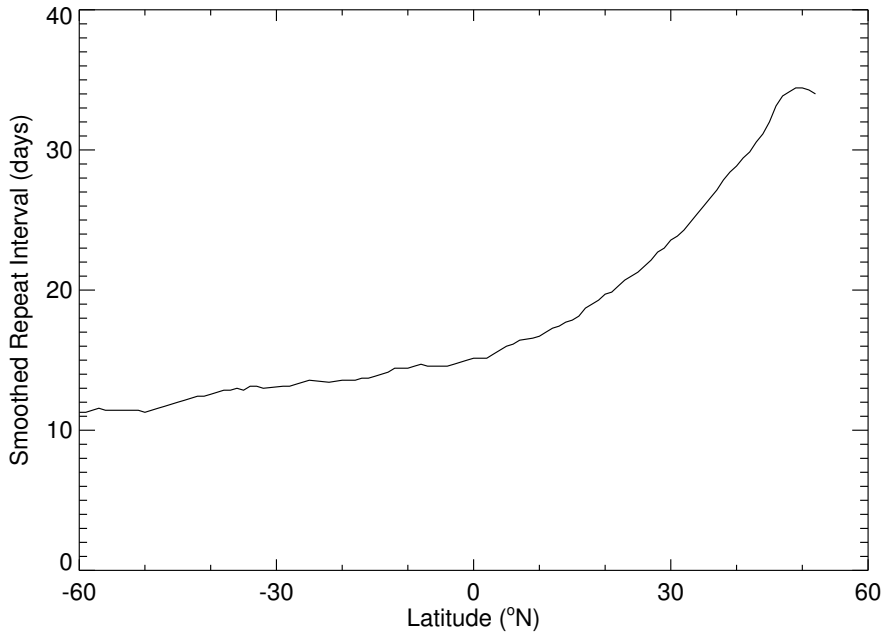

Figure 2.7: Interval between inbound measurements at 130 km altitude at a given latitude and later outbound measurements at the same latitude and altitude from the Daytime Precession part of Phase 2.

at a different altitude, but the same latitude, from the outbound leg of a subsequent aerobraking pass. The precession of periapsis enables me to separate variations due to altitude and latitude despite having non-vertical aerobraking passes. Figure 2.5 shows outbound densities at 130 km altitude between 10°S and 20°S. Orbits whose data are shown in this Figure also measured outbound densities at 140 km, but between 9°S and 18°S. Examining all 140 km outbound data between 10°S and 20°S requires a slightly different set of orbits, and so on for other altitude levels.

Figure 2.8 shows the zonal structure between 10°N and 20°N on the outbound leg during Phase 2 at 130, 140, 150, and 160 km. These data were taken between the 5:1 and 6:1 resonances. I have shifted from 10–20°S to 10–20°N to show the clearest example. The constant density term decreases monotonically as altitude increases, as expected for the background density structure in any atmosphere, and the zonal structure tends to a zonal mean as altitude increases. All the statistically significant peaks and troughs appear fixed in longitude. The trough at 270°E and peak at 330°E are no longer statistically significant at 160 km altitude.

Figure 2.9 shows the normalized harmonic amplitudes, and their uncertainties, from Figure 2.8 as a function of altitude. The normalized amplitudes for the waves-1, 3, and 4 harmonics all decrease as altitude increases. In this example, the normalized amplitude for the wave-2 harmonic does not change in any statistically significant way as altitude increases from 130 km to 160 km. Figure 2.10 shows the phases, and their uncertainties, from Figure 2.8 as a function of altitude. Recall that the maximum value of the phase of the wave-n harmonic is 360°E/n. When the normalized amplitude of the wave-1 harmonic is very small and indistinguishable from zero, its phase is not well-constrained. The phase is meaningless when the amplitude is not significant. All other phases appear constant with altitude.

At 160 km, the individual normalized harmonic amplitudes are about 10%, but the largest peak in the fitted density is 25% greater than the constant density term. This peak normalized amplitude is greater than the 8 – 10% sol-to-sol variability and the similar uncertainty in each density measurement at this altitude.

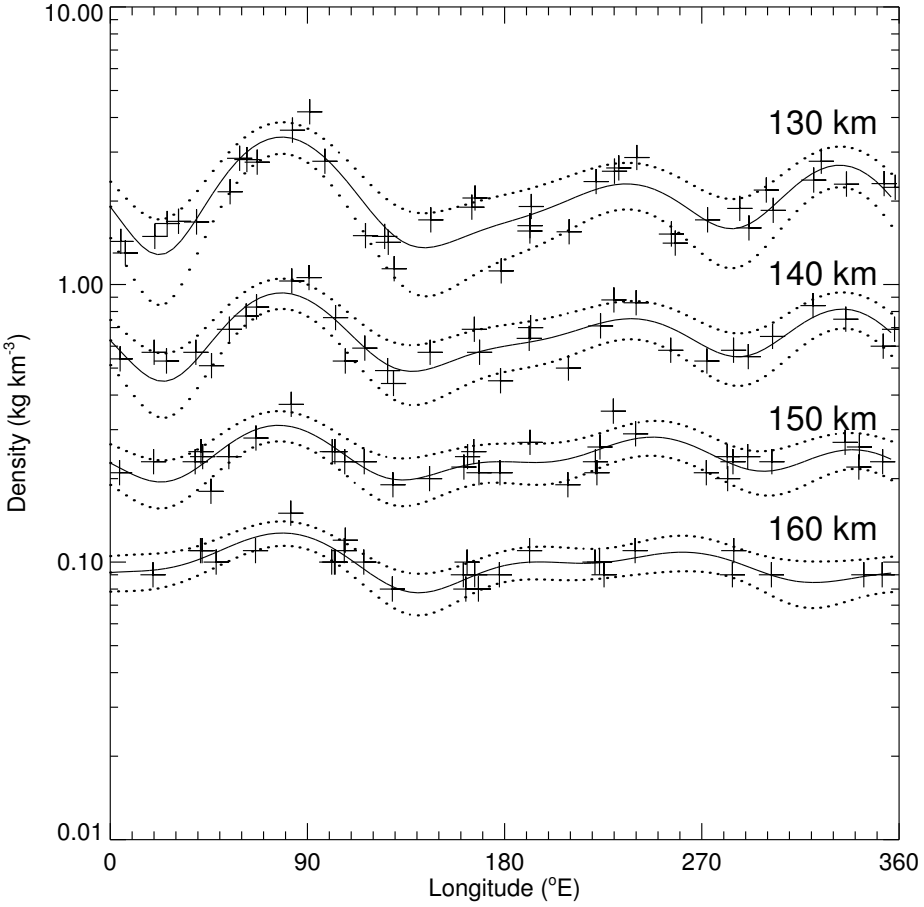

Figure 2.8: Density measurements at 130, 140, 150, and 160 km altitude between 10°N and 20°N for outbound measurements during the Daytime Precession part of Phase 2, plotted as crosses. Model fits to data from each altitude are plotted as solid lines and 1σ uncertainties about each fit as dotted lines. Measurement uncertainties (not shown) are much smaller than the range in multiple measurements at any altitude and longitude. All data were taken at an LST of 15 hrs. Measurements at each altitude level were taken over about a week, but this interval is offset by a couple of days between one altitude level and the next. All density measurements are associated with the obvious altitude level; there are no pathological cases of, say, a 140 km density measurement lurking within the range of the 130 km measurements.

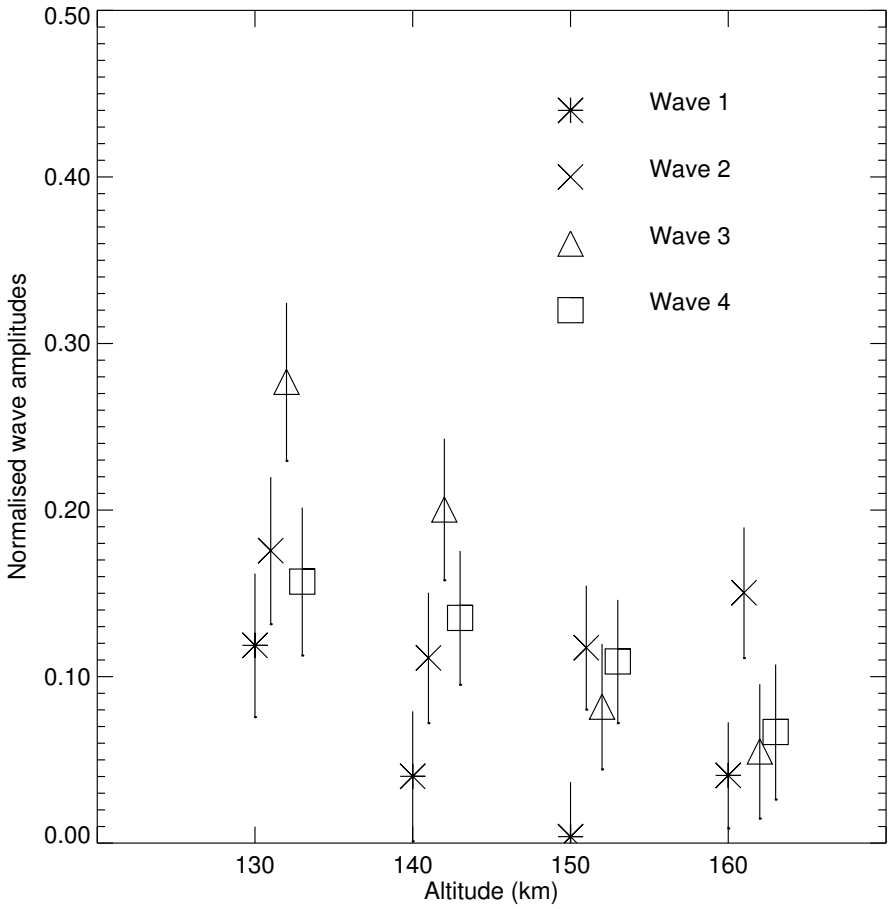

Figure 2.9: Normalized harmonic amplitudes and their uncertainties from Figure 2.8.

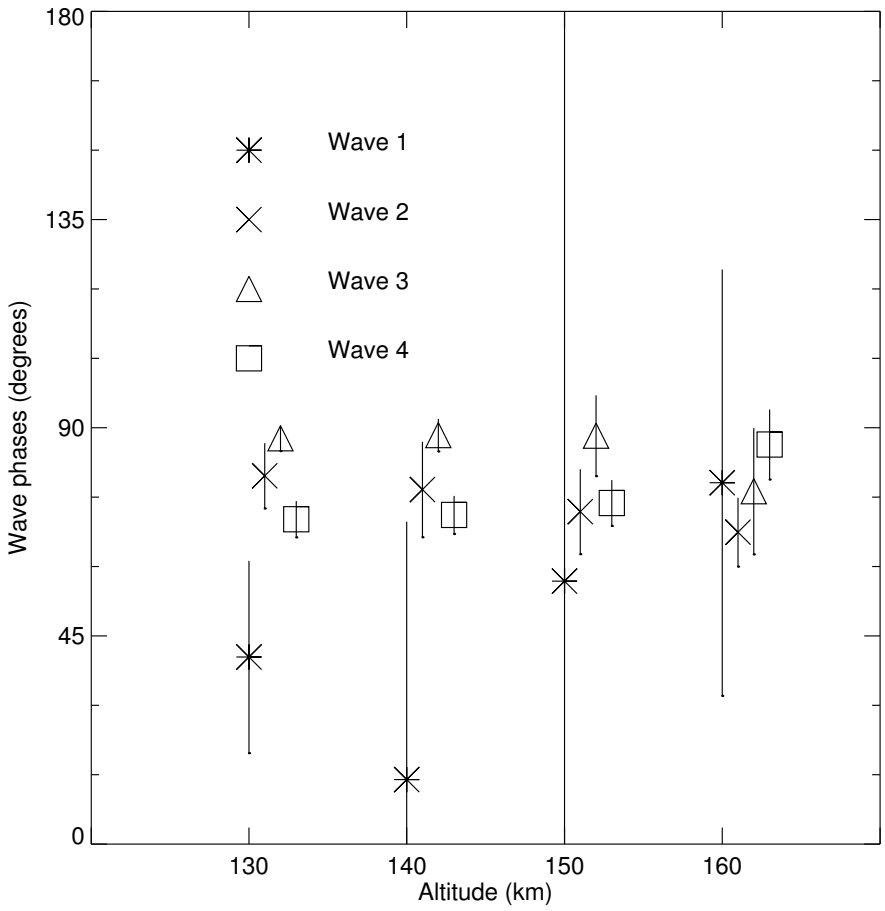

Figure 2.10: Phases and their uncertainties from Figure 2.8.

The similarity of the phases at 160 km to those at lower altitudes supports the contention that I am detecting zonal structure rather than fitting models to noise, but detailed conclusions for this altitude should incorporate the measurement uncertainties and sol-to-sol variabilities in a more formal way. I do not use the 160 km measurements in the remainder of this chapter. At lower altitudes, the zonal structure exceeds the sol-to-sol variability and the measurement uncertainty, both discussed in Section 2.4.1, comfortably.

I have repeated this for other latitude bands between 60°S and 60°N using data from the Daytime Precession part of Phase 2. I generally find that the normalized wave-1 amplitude decreases by about 50% from 130 km to 150 km and those for waves-2, 3, and 4 decrease by about 30%. The rate of change of normalized harmonic amplitude with altitude is influenced by the nature of the atmospheric phenomenon that I observe as zonal structure and are discussed further in Section 2.6.1. Wave-1 normalized amplitudes are small and not very statistically significant at higher altitudes. The phase is meaningless when the amplitude is not significant, which is why its formal value changes erratically with increasing altitude. The wave-2, 3, and 4 phases can change by up to 10–20° with increasing altitude, but are not systematic in an eastward or westward sense within any restricted latitude region and are most consistent with no change in phase with increasing altitude.

Changes in normalized amplitude and phase with increasing altitude are similar at all latitudes. There is no obvious evidence for a shift in behaviour between the northern and southern hemispheres, or between the tropics and extra-tropics. This suggests that the mechanism causing the zonal structure is planetary-scale, rather than localized, and is not restricted to equatorial regions.

Decreases in normalized harmonic amplitude as altitude increases are evidence of dissipation. Classical tidal theory, which assumes a dissipationless medium, predicts that these normalized amplitudes should increase as altitude increases (Chapman and Lindzen, 1970). Possible causes of this dissipation include radiative cooling, wave-wave coupling, shear instabilities, and viscosity (Hooke, 1977;

Forbes, 1995).

Tracadas et al. (2001) modelled the orbit of MGS during the Science Phasing Orbits and found that the zonal structure did not exist in density measurements at 180 km altitude, $L_S = 300° - 30°$, and latitudes north of 60°N at either 07 or 13 hours LST. This is consistent with my observation of decreasing normalized harmonic amplitude with increasing altitude up to 160 km.

Bougher et al. (2001) used data from the MGS Radio Science experiment to find that the altitude of peaks in vertical profiles of electron number density varied systematically with longitude. This zonal structure in electron number density, observed at about 135 km altitude in the primary peak at $64° - 67°$N, $L_S = 70°$, and LST = 04 hours, closely matches that seen in the neutral atmospheric density at $60° - 65°$N, $L_S = 30°$, LST = 16 hours (12 hours offset), and 130 km altitude. Bougher et al. (2001) noted that the longitudes of maxima in the electron number density shifted by about 30° over the 20 km altitude difference between the primary peak near 135 km and the secondary peak near 115 km. The amplitude of their zonal structure is greater at 115 km (8 km peak-to-peak) than at 135 km (6 km peak-to-peak), which is consistent with our observation of decaying normalized harmonic amplitude with increasing altitude. The difference between their apparent observation of a phase shift and my absence of one may be due to limited secondary peak data, the different altitudes, or their restriction to one latitude region poleward of 60°N where different tidal modes may be responsible for the zonal structure. This point is addressed further in Section 2.6.2.

Wilson (2002) used a GCM to model atmospheric densities at 130 km altitude and below. His neutral density results reproduced the amplitude and phase and 30° phase shift observed by Bougher et al. (2001) in electron density. His Figure 3 shows that simulated normalized harmonic amplitudes increase with increasing altitude up to the model top at 130 km, inconsistent with the decrease in amplitude in Bougher et al. (2001).

Hinson et al. (2001) analysed temperature profiles as a function of pressure from 0 – 50 km altitude at latitude = 65°N, 04 hours LST, and $L_S = 74° - 77°$. They observed wave-2 zonal structure in the temperature and geopotential height as functions of pressure at their higher altitudes. Banfield et al. (2000) also observed wave-2 zonal structure in the lower atmosphere. Both observations had temperature amplitudes of about 1K, or 1%.

In summary, the zonal structure is present between 130 and 160 km and decays with increasing altitude. The wave-1 harmonic decays the fastest and the remaining harmonics decay less rapidly (but similar to each other). There are no phase shifts with increasing altitude. The similar behaviour of the zonal structure at all latitudes between 60°S and 60°N suggests a planetary-scale cause. Observations at 115 km and 180 km are consistent with a monotonic decay in the zonal structure between those altitudes. Models have some success at reproducing the 115 km observation of the zonal structure.

2.5.4 Changes in Zonal Structure With Latitude

In this section I examine changes in the normalized amplitudes and phases of each harmonic in the zonal structure as a function of latitude, discuss whether the zonal structure is planetary-scale or localized, and quantify which harmonics are dominant.

In Section 2.5.1 I built up a picture of the zonal structure at 130 km using outbound data. In order to sample enough longitudes I had to include data from so many orbits that the measurement latitude precessed from 10°S at the first density measurement to 20°S at the last density measurement. By allowing periapsis latitude (and the latitude corresponding to the measurement altitude) to precess still further, I can see how the zonal structure changes from one latitude range to another.

Figure 2.11 shows the zonal structure as a function of latitude for inbound

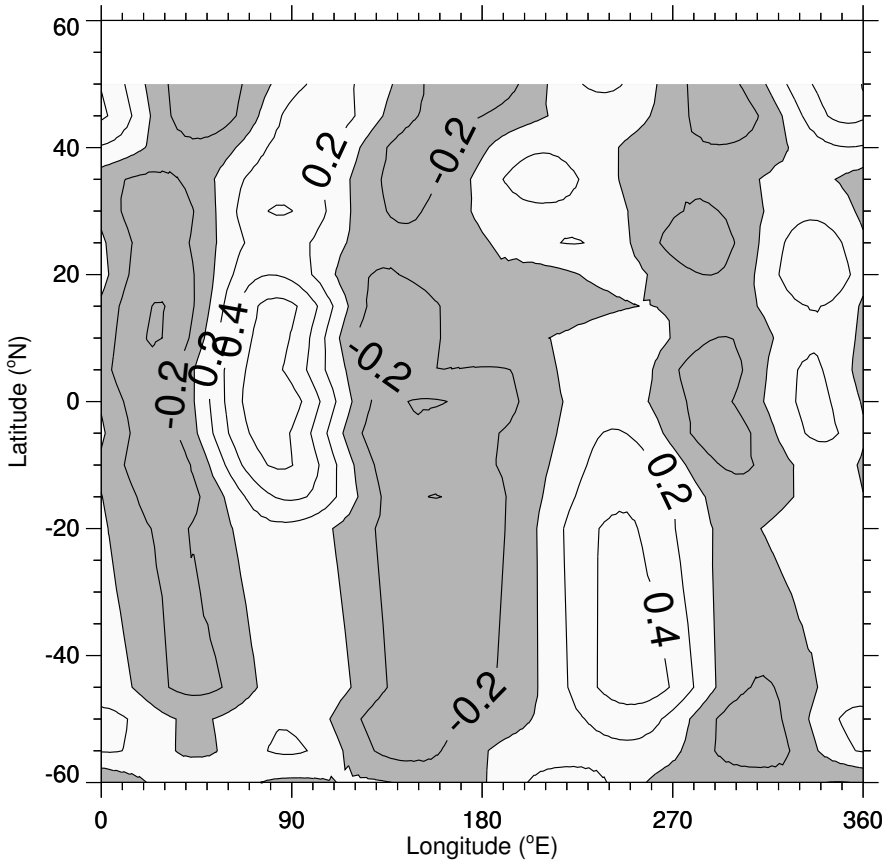

Figure 2.11: Contour plot of (fitted density – constant density term) / (constant density term) at 130 km altitude, inbound leg, from the Daytime Precession part of Phase 2. The normalization highlights the zonal structure. The LST of the data is 17 hrs in the north, decreasing to 15 hrs in the south. The L_S of the data is 30° in the north, increasing to 80° in the south. Contour intervals are 0.2 (dimensionless) and negative regions (low densities) are shaded. The peaks and troughs from Figure 2.6 can be seen between 10°S and 20°S.

data at 130 km altitude from the Daytime Precession part of Phase 2. Wavefits similar to Figure 2.6 were constructed at five degree intervals with ten degree windows in latitude. The difference between the wavefit and the constant density term as a function of longitude was then normalized by the constant density term, and these values were then merged into a contour plot. There is overlap between adjacent latitude windows, so adjacent wavefits are not statistically independent. The overlap is included to smooth the contours. Figure 2.11 should be compared to Figure 1 of Wilson (2002) which uses both inbound and outbound data. The two Figures are similar, as they should be according to Section 2.5.2. Only wavefits from latitude ranges which yielded a good fit, as discussed in Section 2.5.1, are included in this plot. Latitude ranges with bad fits, 20–40°S, include orbits 911–961 which have poor or missing data due to spacecraft computer problems. Since zonal fits in this range are poor because of inadequate data, this region in Figure 2.11 is filled by the interpolation of nearby fits. Uncertainties in the fitted density as a function of latitude and longitude are not shown, but the mean 1σ uncertainty is 20% of the constant density term with most values within a few percentage points of this mean. Figure 2.6 shows the uncertainty in the fit in one latitude range.

A contour plot similar to Figure 2.11, but using outbound data, can also be constructed. Measurements at a given altitude and latitude are taken first on the inbound leg and then, a few weeks later, on the outbound leg. A contour plot similar to Figure 2.11, but at a different altitude, can also be constructed. There is also a few days difference in time between measurements at a given latitude and different altitudes. All these similar contour plots have a high density peak at 80°E, most prominent in the northern hemisphere, a high density peak at 250°E, most prominent in the southern hemisphere, and a high density peak at 330°E. The peak at 330°E is always the smallest and the other two peaks are relatively large.

The meridionally broad nature of the zonal structure is immediately apparent. Together with its stability on fortnightly timescales, discussed in Section 2.5.2,

and its consistent behaviour with altitude at different latitudes, discussed in Section 2.5.3, this implies that whatever atmospheric phenomenon is causing the zonal structure operates on a planetary scale. At first glance, given the two large peaks 180 degrees apart, the wave-2 harmonic appears dominant.

Figures 2.12 and 2.13 show the normalized amplitudes and phases of the harmonic fit displayed in Figure 2.11 over a range of latitudes. The situation is more complicated than a mere wave-2 dominance. Wave-3 is dominant in the northern extratropics and no single harmonic is dominant in the southern extratropics or the tropics. Wave-1 is the weakest harmonic over the entire range of latitude. Waves-2, 3, and 4 all have phases, all around 90°E, which stay remarkably constant over a wide range of latitude. This constancy is additional evidence that a planetary-scale mechanism is responsible for the zonal structure. Similar conclusions are reached from the study of outbound data and/or different altitudes.

Figures 2.14 and 2.15 show the wave-2 and wave-3 components of Figure 2.11. They should be compared to Figures 2a and 2b of Wilson (2002). The two pairs of Figures are similar, as they should be according to Section 2.5.2. The constancy of the phases can be seen, as can the way in which these two harmonics interfere to yield the apparent wave-2 dominance in Figure 2.11. Overlaps between peaks in the wave-2 and wave-3 harmonics (*i. e.* constructive interference to give large densities) occur at about 80°E (mainly in the northern hemisphere) and 250°E (mainly in the southern hemisphere). The wave-3 peak at 330°E destructively interferes with the wave-2 trough at the same longitude to give only a small peak in density. The shift in the phase of the wave-3 harmonic with latitude is responsible for the shift of the largest peak in the zonal structure from 80°E in the northern hemisphere to 250°E in the southern hemisphere.

Figure 2.12 shows erratic changes in normalized harmonic amplitude with latitude, in contrast to the well-behaved phases of Figure 2.13. This may represent the individual responses by each tidal mode to whatever surface inhomogeneity is

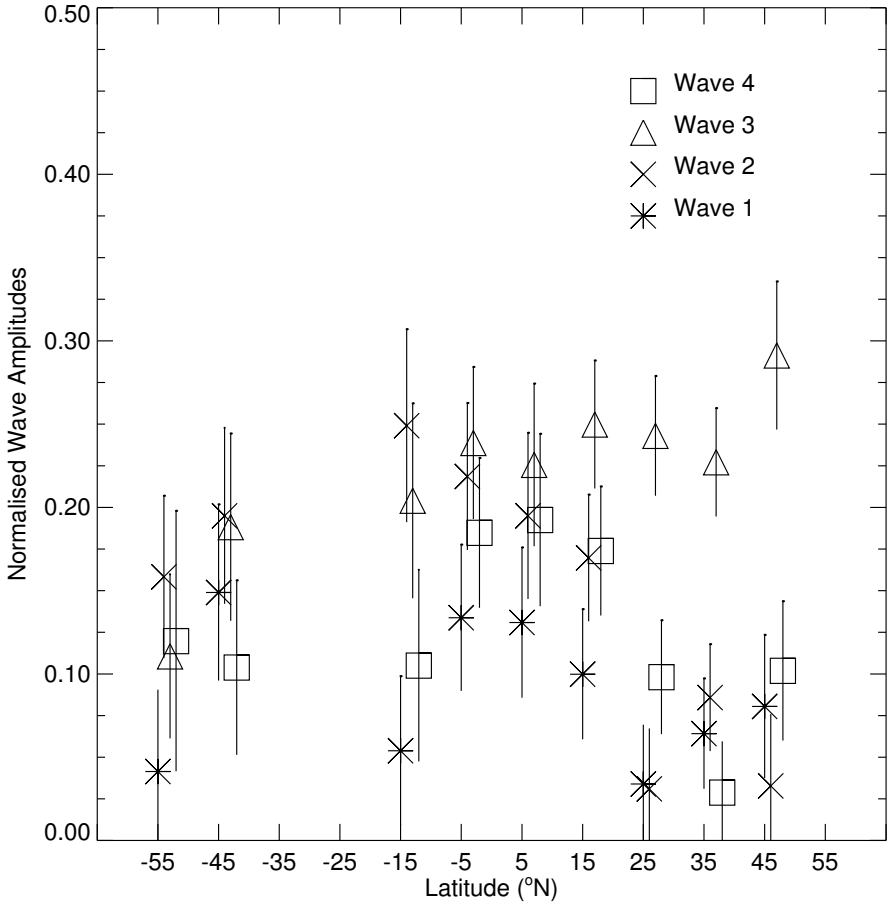

Figure 2.12: Normalized amplitudes from the wave-4 harmonic fits that were merged to create Figure 2.11. The latitude of each set of harmonics is the centre of the 10° wide latitude band from which all the density measurements that contributed to the harmonic fit came. Only every other fit used in Figure 2.11 is shown; including every fit increases the clutter without aiding interpretation. Gaps at 25°S and 35°S are due to bad fits which were not included in Figure 2.11.

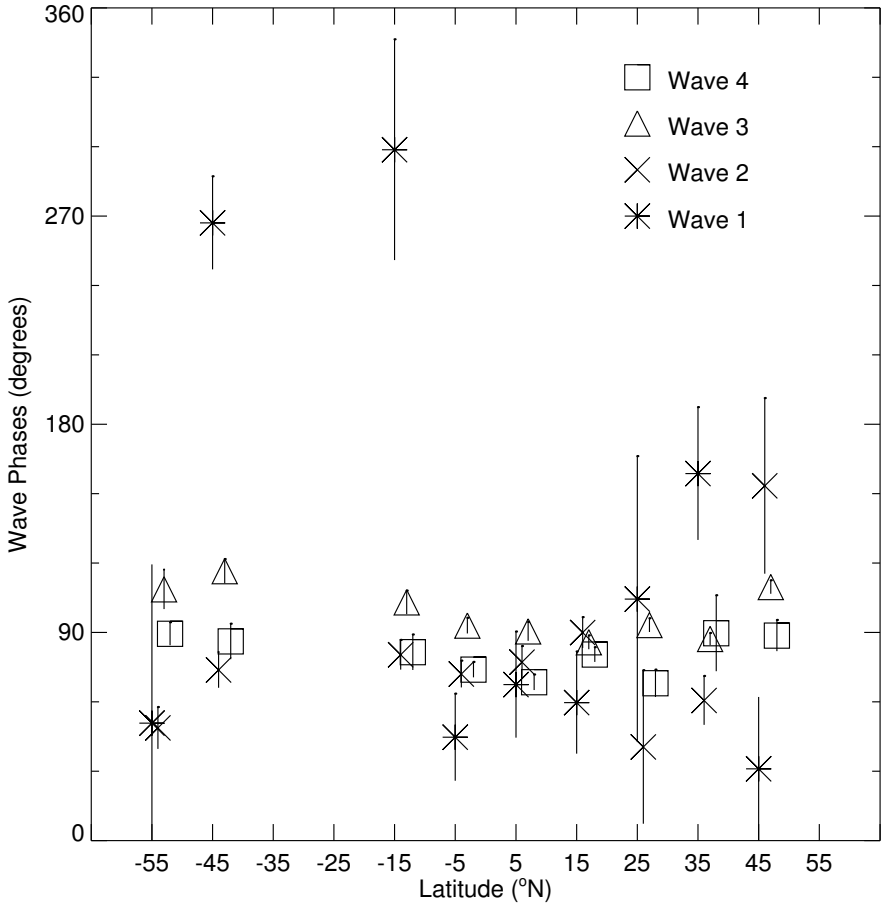

Figure 2.13: Phases corresponding to the amplitudes in Figure 2.12. Recall that the maximum value of the phase of the wave-n harmonic is $360°\mathrm{E}/n$.

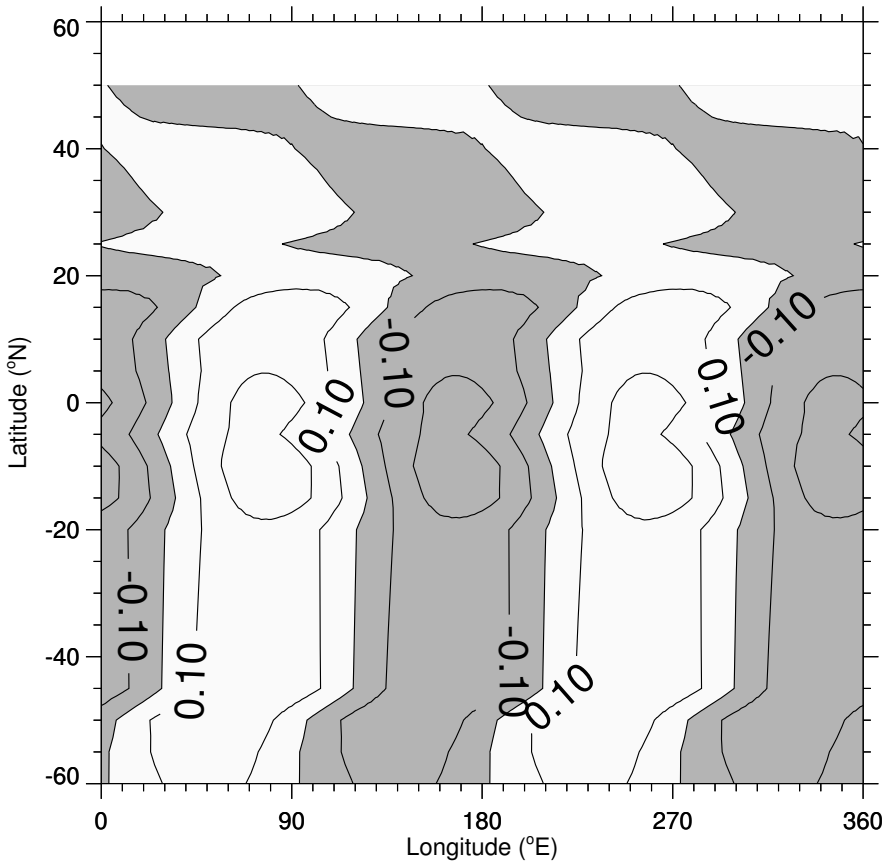

Figure 2.14: As Figure 2.11, but plotting only the wave-2 components. Contour intervals are 0.1 and negative regions (low densities) are shaded.

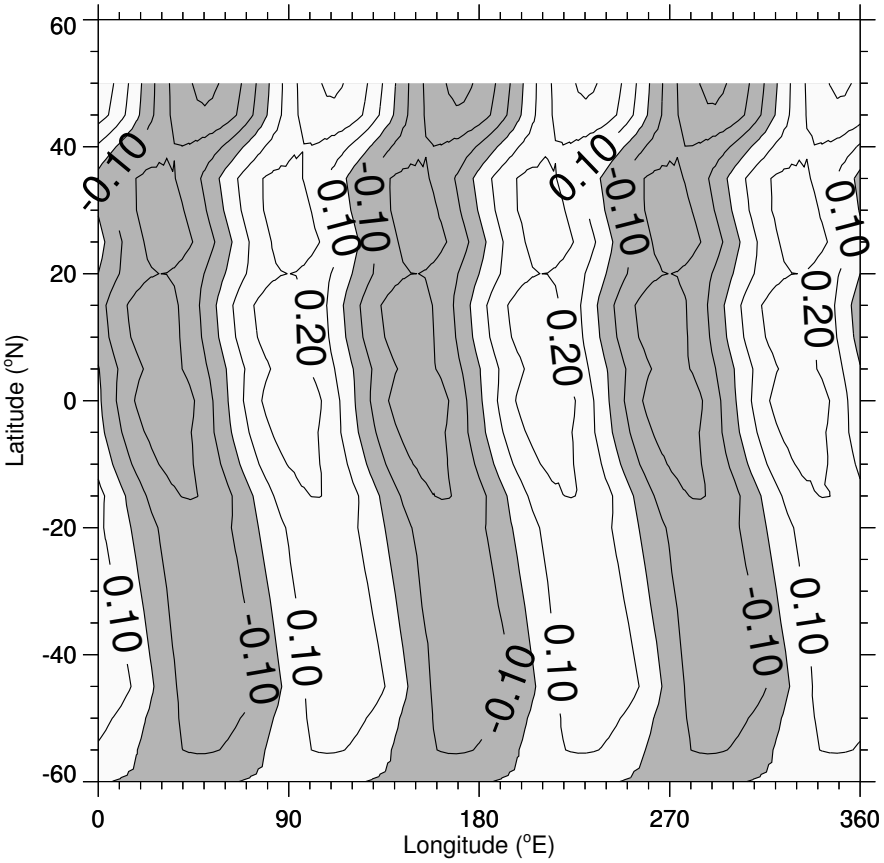

Figure 2.15: As Figure 2.11, but plotting only the wave-3 components. Contour intervals are 0.1 and negative regions (low densities) are shaded.

causing the zonal structure and/or the ease of propagation through the lower atmosphere at this latitude. Insight into this behaviour may come from new surface-to-thermosphere GCMs currently under development (Bougher et al., 2002; Angelats i Coll et al., 2002).

The total energy associated with each harmonic in a given latitude band is proportional to the product of the area of the latitude band and the square of the amplitude. A measure of the global strength of each harmonic is its root-mean-square (rms) normalized amplitude, where the mean-square normalized amplitude has been weighted by the cosine of latitude. Using both inbound and outbound harmonic amplitudes at 130 km altitude, I find that the wave-3 rms normalized amplitude of 22% is greatest. Wave-2 is the next strongest at 18%, followed by wave-4 at 14%, and wave-1 at 12%. The 1σ uncertainties in the rms normalized amplitudes are 1%. Wave-2 is not the most important harmonic in the observed zonal density structures; wave-3 is.

Wilson (2002) used a GCM to model atmospheric densities at 130 km altitude and below. He found wave-2 and wave-3 to be the strongest harmonics at 120 km altitude, with wave-2 stronger than wave-3, and reproduced the lack of phase variation with changes in latitude.

In summary, the zonal structure is meridionally broad, suggesting a planetary-scale cause. This is in contrast to the sol-to-sol variability, which has a smaller meridional length scale. The phases of individual harmonics in the zonal structure are stable, often around 90°E, yet their normalized amplitudes are erratic. Wave-3 is the dominant harmonic, followed by wave-2. Models are broadly able to reproduce the observations.

2.5.5 Changes in Zonal Structure With Local Solar Time

In this section I use data from the Polar Crossing part of Phase 2 of aerobraking to examine the week-to-week repeatability of the zonal structure in polar regions,

then compare the normalized amplitudes and phases of harmonics in dayside and nightside zonal structures in polar regions.

During the Daytime Precession part of Phase 2, periapsis latitude precessed southward with little change in periapsis LST from one orbit to the next, little change in longitude from atmospheric entry to exit during an individual aerobraking pass, and little change in LST from atmospheric entry to exit during an individual aerobraking pass. This is shown in Figure 2.1. Periapsis cannot continue to precess southward indefinitely. As periapsis continued to precess around in the orbital plane, it reached an extreme southern latitude, then precessed northward. Periapsis, which was on the sunward, daytime side of Mars, has shifted to the antisunward, nighttime side of Mars. The extreme southern latitude ($\sim$ 87°S) is set by the inclination of MGS's orbital plane. Since periapsis crossed the terminator during this Polar Crossing, periapsis LST must change from one orbit to the next.

As in the Daytime Precession part of Phase 2, periapsis longitude changes from one orbit to the next during this Polar Crossing. Unlike the Daytime Precession behaviour, the longitude of MGS during an individual aerobraking pass also changes during this Polar Crossing. The longitude of MGS must steadily track through all 360° during one orbit. At polar latitudes, MGS's longitude changes significantly over short arcs of an orbit as MGS crosses the converging lines of longitude. When periapsis occurs close to the pole, MGS's longitude changes significantly over the short arc that is the aerobraking pass. MGS's LST changes significantly during an individual aerobraking pass for exactly the same reason.

As periapsis precesses southwards towards the pole, the 130 km altitude level on the inbound leg occurs to the south of periapsis and periapsis occurs to the south of the 130 km level on the outbound leg. That is, MGS travelled from south to north during an aerobraking pass before reaching its furthest south. The 130 km altitude level on the inbound leg reaches its furthest south, crosses the terminator from day to night, and moves northward before periapsis does. Periapsis, in turn, does so before the 130 km altitude level on the inbound leg. When periapsis was

at its furthest south, MGS travelled from north to south on the inbound leg, then from south to north on the outbound leg.

When periapsis is exactly at its furthest south, the latitudes at which the inbound and outbound legs cross, say, the 130 km altitude level are the same. This is a consequence of the reflection symmetry of an ellipse (such as an orbit) about its semi-major axis. With a near-polar orbit, the LSTs of these two points are about half a sol apart. Density measurements can be made a few minutes apart at exactly the same latitude and altitude, half a sol apart in LST. By considering several orbits close to when periapsis was at its furthest south, a picture of the daytime and nighttime zonal structure at a given altitude and this latitude can be built up.

In practice, to accumulate enough data to build up a picture of the zonal structure at, say, 130 km takes so many orbits to acquire that there is a finite range in the latitude of the measurements (as in Section 2.5.1). I use a 20° wide latitude range, instead of the usual 10°, because there are fewer measurements per degree of latitude at this stage of aerobraking than before.

When periapsis is at its furthest south, the inbound and outbound legs cross the 130 km altitude level at about 70°S. At this time, the 130 km altitude level on the inbound leg is moving north and the same altitude level on the outbound leg is moving south. To build up a picture of the zonal structure at 130 km between 50°S and 70°S, I must use data from the preceding week for the outbound case and data from the following week for the inbound case. Despite this difference of about a week between the two sets of observations at 50–70°S, can I compare them as if they were taken simultaneously? I addressed this problem for non-polar regions in Section 2.5.2 and found that I could do so. Here I should examine the week-to-week repeatability of both the daytime and the nighttime zonal structure. I would like to compare daytime measurements at 130 km between 50°S and 70°S for inbound and outbound legs. I would also like to compare nighttime measurements at 130 km between 50°S and 70°S for inbound and outbound legs. However, aerobraking

ended when the 130 km altitude level on the outbound leg reached its furthest south and repeat nighttime measurements are not available.

There are three relevant subsets of data at 130 km altitude between 50°S and 70°S; inbound on the dayside with MGS travelling from south to north through the atmosphere, outbound on the dayside with MGS travelling from south to north through the atmosphere, and inbound on the nightside with MGS travelling from north to south through the atmosphere. Due to the cold temperatures and consequently decreased densities, nightside data at higher altitudes are not available in useful quantities. Figure 2.16 shows the intervals between these three sets of measurements at a given latitude. In the 50–70°S latitude band, the 11 day interval between inbound dayside and outbound dayside measurements is longer than the interval between inbound nightside and outbound dayside measurements. The difference in LST between the nightside measurements at LST = 02 hours and the dayside measurements at LST = 15 hours is very close to half a sol. Figures 2.17, 2.18, and 2.19 show wavefits for the three sets of measurements at 130 km altitude between 50°S and 70°S. Each of the three includes a couple of resonances, the 8:1 and 9:1 for inbound on the dayside, the 10:1 and 11:1 for outbound on the dayside, and the 11:1 and 12:1 for inbound on the nightside. The normalized amplitudes and phases of the various harmonics are shown in Table 2.3. A comparison between the inbound dayside and outbound dayside results is consistent with the results of Section 2.5.2 for more equatorial latitudes — changes in normalized amplitudes and phases are minor.

Assuming that the nightside atmosphere does not change more rapidly than the dayside atmosphere does, I can compare the phases of the inbound nightside and outbound dayside wavefits as if the measurements were effectively simultaneous. There is no way to test this assumption with the MGS accelerometer data. The formal amplitude of each of the four harmonics has increased from day to night, but with little statistical significance. The phase of the wave-1 harmonic changes by approximately 90 degrees, the phase of the wave-2 harmonic changes by

Parameters	Inbound Dayside	Outbound Dayside	Inbound Nightside
Constant Amplitude (kg km^{-3})	0.807 ± 0.023	0.810 ± 0.027	0.383 ± 0.033
Normalized Wave 1 Amplitude	0.069 ± 0.040	0.083 ± 0.047	0.275 ± 0.125
Normalized Wave 2 Amplitude	0.148 ± 0.041	0.168 ± 0.046	0.280 ± 0.115
Normalized Wave 3 Amplitude	0.066 ± 0.040	0.134 ± 0.046	0.202 ± 0.118
Normalized Wave 4 Amplitude	0.051 ± 0.049	0.101 ± 0.048	0.126 ± 0.139
Wave 1 Phase (degrees)	154.8 ± 33.0	207.1 ± 32.2	107.7 ± 24.2
Wave 2 Phase (degrees)	52.4 ± 7.6	37.1 ± 8.2	117.0 ± 12.4
Wave 3 Phase (degrees)	108.3 ± 11.5	117.3 ± 6.7	114.8 ± 10.8
Wave 4 Phase (degrees)	3.4 ± 10.2	85.4 ± 6.4	88.9 ± 11.4

Table 2.3: Model fit parameters for measurements made at 130 km between 50–70°S during Phase 2. Uncertainties are 1σ.

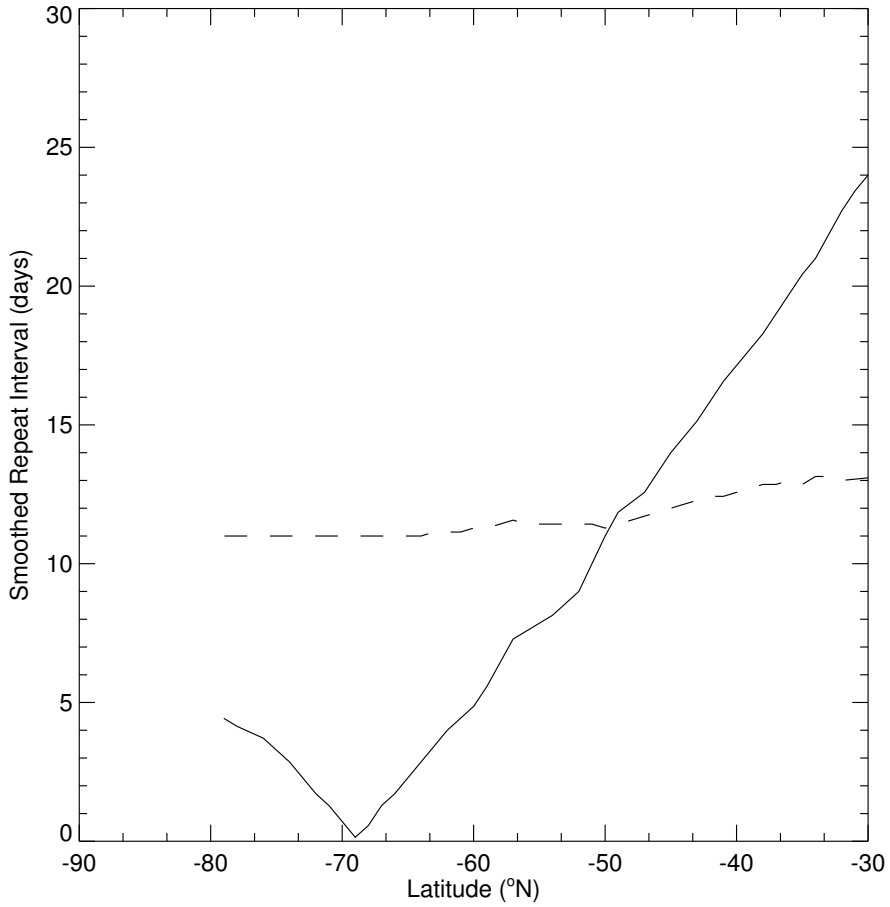

Figure 2.16: Interval between outbound dayside measurements at 130 km altitude and a given latitude and inbound nightside measurements at the same latitude and altitude (solid line) from Phase 2. The minimum near 70°S occurs when periapsis is at its furthest south. At more northern latitudes, outbound dayside measurements preceed inbound nightside measurements. At more southern latitudes, inbound nightside measurements preceed outbound dayside measurements. Also plotted is the interval between outbound dayside measurements at 130 km altitude and a given latitude and inbound dayside measurements at the same latitude and altitude (dashed line) from Phase 2. Inbound dayside measurements always preceed outbound dayside measurements. South of 50°S, the interval between day-night repeat measurements at a given latitude and 130 km altitude is less than that between day-day repeat measurements at that latitude and altitude.

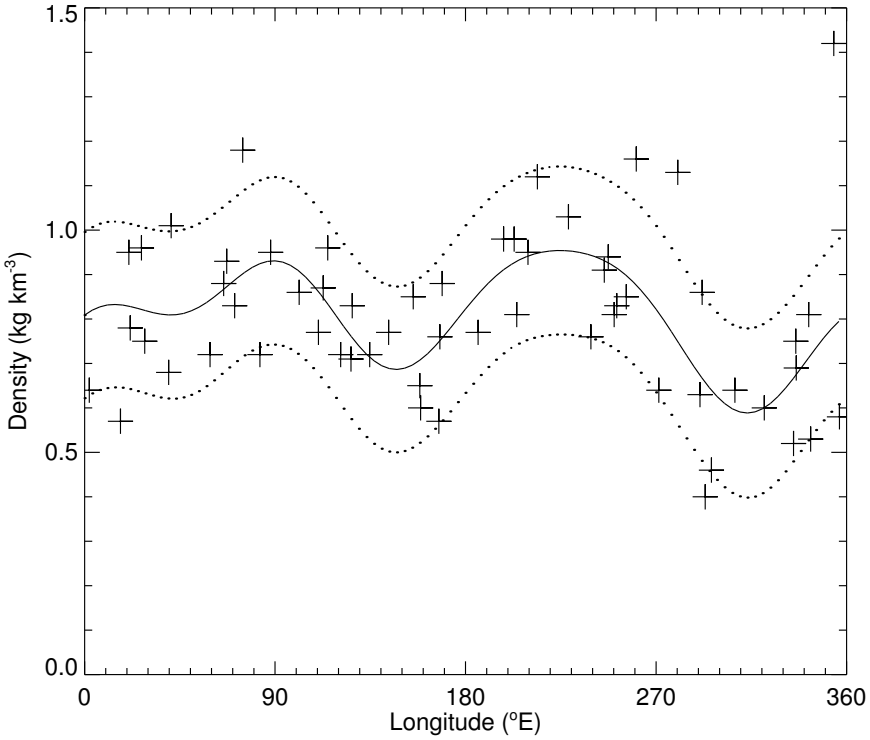

Figure 2.17: All inbound dayside density measurements at 130 km altitude between 50°S and 70°S from Phase 2, crosses, wave-4 harmonic model fit to the data, solid line, and 1σ uncertainties about the fit, dotted lines. The data were collected over about a week, all at an LST of 15 hrs. Measurement uncertainties (not shown) are much smaller than the range in multiple measurements at any longitude. The zonal structure is less pronounced than in Figure 2.5 or others from the tropics, but is still significant above a zonal mean.

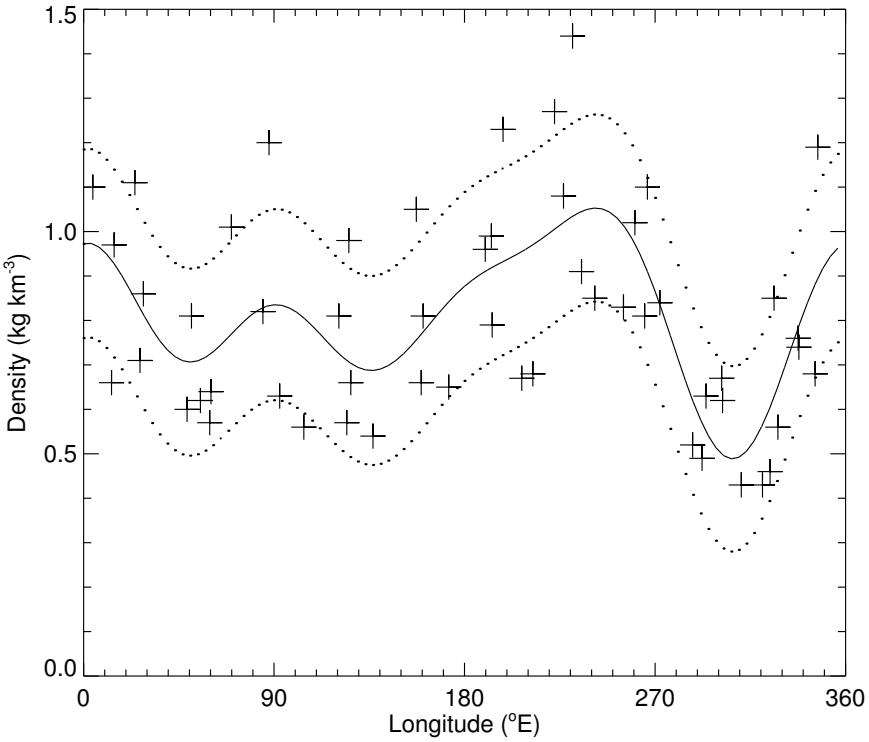

Figure 2.18: As Figure 2.17, but using outbound dayside density measurements. The data used here were collected about 11 days after those in Figure 2.17, but the weak zonal structure is still broadly the same.

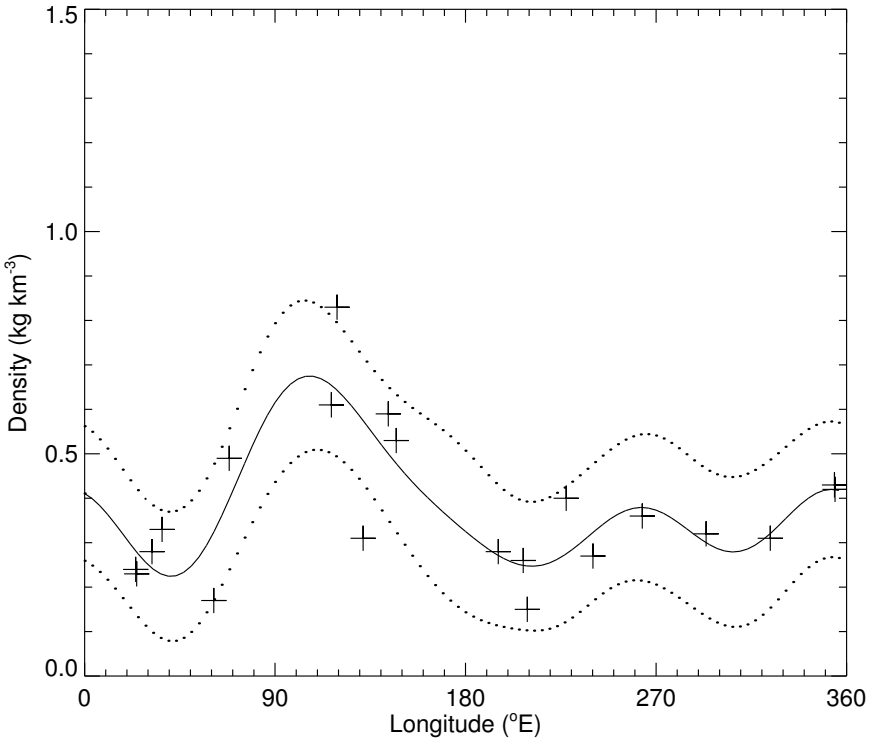

Figure 2.19: As Figure 2.17, but using inbound nightside density measurements. The LST is 02 hrs. Densities have decreased from day to night, and the zonal structure is very different.

approximately 90 degrees, and the phase of the wave-3 harmonic does not change. The wave-4 harmonic is not statistically significant in the nightside wavefit. These phase changes have implications for the nature of the atmospheric phenomenon that I observe as zonal structure and is discussed further in Section 2.6.1.

Bougher et al. (2001) found evidence for a zero phase shift in a wave-3 zonal density harmonic at 64–67°N between 04 and 16 hours LST in their comparisons of electron and neutral density, but did not present a detailed harmonic breakdown.

In summary, the stability of zonal structure is similar in the polar regions and in the tropics and the phases of some harmonics in the zonal structure in the polar regions change with half a sol change in LST.

2.6 Modelling of the Zonal Structure

2.6.1 Constraints on Tidal Modes Responsible for Zonal Structure

The zonal structures observed in the martian upper atmosphere can be studied using tidal theory. "Atmospheric tides are global-scale oscillations in temperature, wind, density, and pressure at periods which are subharmonics of a solar or lunar day" (Forbes, 1995). The dominant forcing in the martian atmosphere is solar heating. My aim in this section of the chapter is to use only the accelerometer data and classical tidal theory to initially identify which σ, s tidal modes are causing the zonal structure in the upper atmosphere. Previous observations and theory that relate to this are discussed in Section 2.6.2 when I re-examine the preliminary conclusions of this section.

Tidal variations in density at fixed altitude, latitude and season with dependence on longitude and LST can be represented as (Chapman and Lindzen, 1970; Forbes and Hagan, 2000; Wilson, 2000a)

$$\rho\left(\lambda, t_{LST}; z, \theta, L_S\right) = \qquad (2.1)$$

$$\sum_{\sigma,s} \rho_{\sigma,s}\left(z,\theta,L_S\right)\cos\left(\sigma\Omega\left(t_{LST}-\lambda/2\pi\right)+s\lambda-\phi_{\sigma,s}\left(z,\theta,L_S\right)\right)$$

where ρ is density, λ is east longitude, t_{LST} is local solar time in sols, z is altitude, θ is latitude, L_S is heliocentric longitude or season, σ is the temporal harmonic ($\sigma = 0, 1, 2, \ldots$), s is the zonal wavenumber ($s = \ldots, -2, -1, 0, 1, 2, \ldots$), $\Omega = 2\pi$ sol^{-1}, and $\phi_{\sigma,s}$ is the phase.

Westward propagating tides have $s > 0$, eastward propagating tides have $s < 0$, and zonally-symmetric tides have $s = 0$. Migrating tides, which have $s = \sigma$, have zonal phase speeds equal to that of the Sun as seen by a fixed observer (Forbes and Hagan, 2000). Non-migrating tides have $s \neq \sigma$. Only migrating tides are excited in a zonally-symmetric atmosphere with zonally-symmetric boundary conditions. If asymmetries are present in the atmospheric boundary conditions, such as albedo, thermal inertia, or topography, then their interactions with the migrating tides generate non-migrating tides (Forbes et al., 1995; Forbes and Hagan, 2000). Zonal inhomogeneities distributed throughout the lower atmosphere, such as dust loading, can also generate non-migrating tides. The non-migrating tides excited by asymmetries of the form $\cos\left(m\lambda - \phi_m\right)$, where m is the zonal wavenumber of the asymmetry, are (Forbes and Hagan, 2000)

$$\rho\left(\lambda, t_{LST}; z, \theta, L_S\right) = \tag{2.2}$$
$$\sum_{\sigma,m} \rho_{\sigma,m}\left(z,\theta,L_S\right)\cos\left(\sigma\Omega t_{LST} \pm m\lambda - \left(\phi_\sigma\left(z,\theta,L_S\right) \pm \phi_m\right)\right)$$

Migrating tides, which are not excited by any asymmetry and have $m = 0$, have no variation with longitude at fixed t_{LST}. The variation with longitude of a non-migrating tide is the same as that of the zonal asymmetry that generated it, but is independent of the temporal harmonic and zonal wavenumber of the migrating tide that generated it.

Solar heating is well described by a combination of diurnal ($\sigma = 1$) and semidiurnal ($\sigma = 2$) harmonics. When the migrating diurnal and semidiurnal tides interact with an $m = 1$ asymmetry, such as topography, they are modulated to

form the $s = 0$ and $s = 2$ diurnal tides and the $s = 1$ and $s = 3$ semidiurnal tides respectively (Forbes and Hagan, 2000). All four of these non-migrating tidal modes appear as zonal variations with wavenumber 1 as seen from the fixed LST reference frame of MGS. Each of the zonal harmonics identified in the accelerometer dataset at fixed LST is influenced by a near-surface asymmetry with the same zonal wavenumber and could be attributable to four possible tidal modes. When I observe a harmonic in the accelerometer dataset, which of the four possible tidal modes is responsible?

I first use classical tidal theory to discuss the behaviour with altitude and latitude of a specific σ, s tidal mode, then reject tidal modes that are not efficiently excited by solar heating, and finally reject those that cannot propagate to the upper atmosphere.

In the classical tidal theory of a highly idealized atmosphere, each σ, s tidal mode can be decomposed into a complete, orthogonal set of functions, called Hough modes (Chapman and Lindzen, 1970). Hough modes are eigenfunctions of the Laplace tidal equation and are labelled with an index n. Conventionally, n may be positive or negative, but not zero, and its absolute value must be greater than or equal to that of s. The meridional structure of each σ, s, n Hough mode is separable from its vertical structure. Note that I refer to a disturbance with a given temporal and zonal structure as a σ, s tidal mode and to one with a given temporal, zonal, meridional, and vertical structure as a specific σ, s, n Hough mode.

Roughly speaking, the meridional structure of a specific σ, s, n Hough mode determines whether it is efficiently excited by solar heating and its vertical structure determines whether it is able to propagate to the upper atmosphere. If none of the σ, s, n Hough modes that make up a given σ, s tidal mode can be efficiently excited by solar heating *and* propagate to the upper atmosphere, then that σ, s tidal mode cannot influence the accelerometer measurements of the zonal structure.

I discuss the meridional structure of Hough modes and their excitation by

solar heating, then discuss the vertical structure of Hough modes and their vertical propagation.

Hough modes are either symmetric or asymmetric about the equator. Those that are symmetric about the equator are either peaked at the equator or poleward of the tropics. For given values of σ and s, the larger the absolute value of n, the more nodes (latitudes at which the value of the Hough mode is zero) the Hough mode has. For a σ, s, n Hough mode to contribute strongly to the zonal structure in the upper atmosphere, it must be efficiently excited by solar heating. Like solar heating, it must be symmetric about the equator, be peaked at the equator rather than poleward of the tropics, and have no nodes too close to the equator. A σ, s, n Hough mode which does not satisfy these excitation criteria is not be efficiently excited by solar heating. Figure 2.20 shows 8 Hough modes with $\sigma = 1, s = -1$. They are all possible causes of the observed wave-2 zonal structure in the upper atmosphere. n ranges from 1 to 4 and from -1 to -4. Only one of the modes, $n = 1$, comes close to satisfying the above excitation criteria. It is the first (*i. e.* lowest absolute value of n) symmetric mode for this σ, s combination. For each of the 16 σ, s tidal modes that could cause wave-1 to wave-4 harmonics in the accelerometer dataset, only the first symmetric σ, s, n Hough mode satisfied the excitation criteria. The first symmetric, diurnal, and eastward propagating Hough mode for a given zonal wavenumber $-s$ is called a diurnal Kelvin wave and labelled as DKs. The $\sigma = 1, s = -1, n = 1$ mode that satisfies the excitation criteria above is DK1.

In the idealized case of classical tidal theory, a Hough mode propagates vertically as either an evanescent or a travelling wave (Chapman and Lindzen, 1970). In reality, damping in the martian atmosphere is quite strong for even the travelling waves (Zurek et al., 1992; Forbes et al., 2001). Figure 2.21 shows the vertical wavelengths of the 16 σ, s, n Hough modes that satisfied the above excitation criteria. An altitude of 130 km, representative of the accelerometer dataset, corresponds to about 15 scale heights above the martian surface. All the evanescent Hough modes in Figure 2.21 should propagate to this altitude with minimal damping, since their

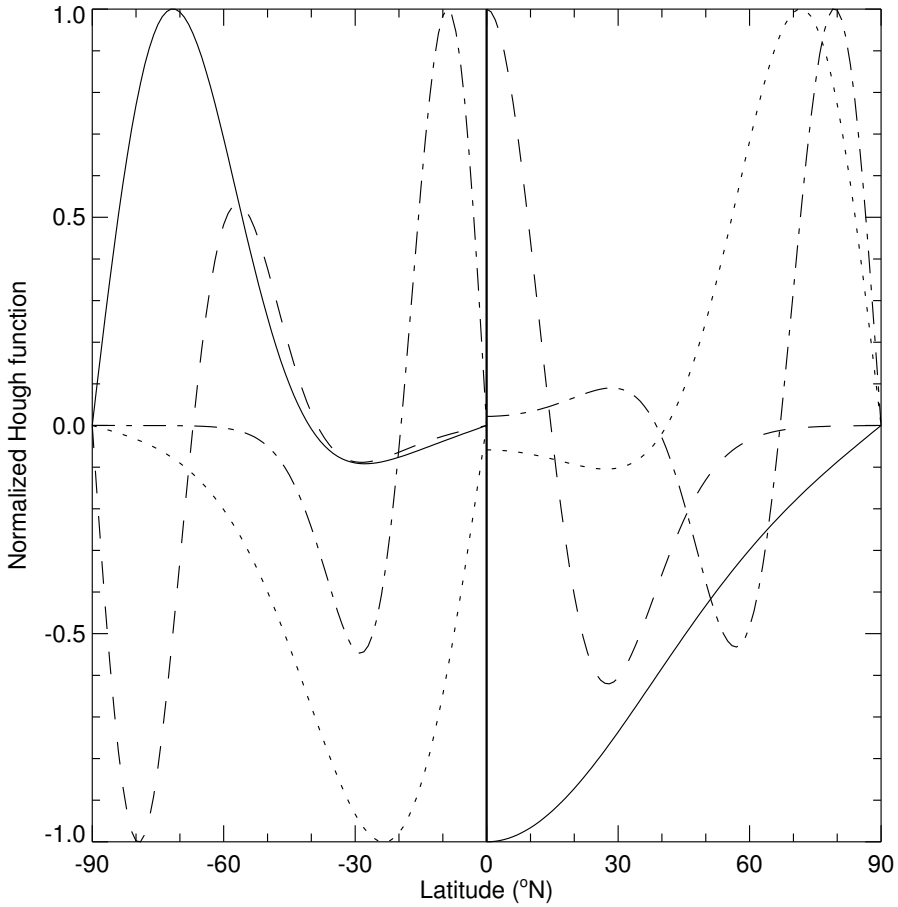

Figure 2.20: Meridional structure of the eight lowest order Hough modes with $\sigma = 1, s = -1$. Asymmetric functions are shown in the southern hemisphere only, symmetric functions are shown in the northern hemisphere only. Asymmetric functions are $n = -1$ (solid line), $n = 2$ (dotted line), $n = -3$ (dashed line), $n = 4$ (dot-dash line). Symmetric functions are $n = 1$ (solid line), $n = -2$ (dotted line), $n = 3$ (dashed line), $n = -4$ (dot-dash line).

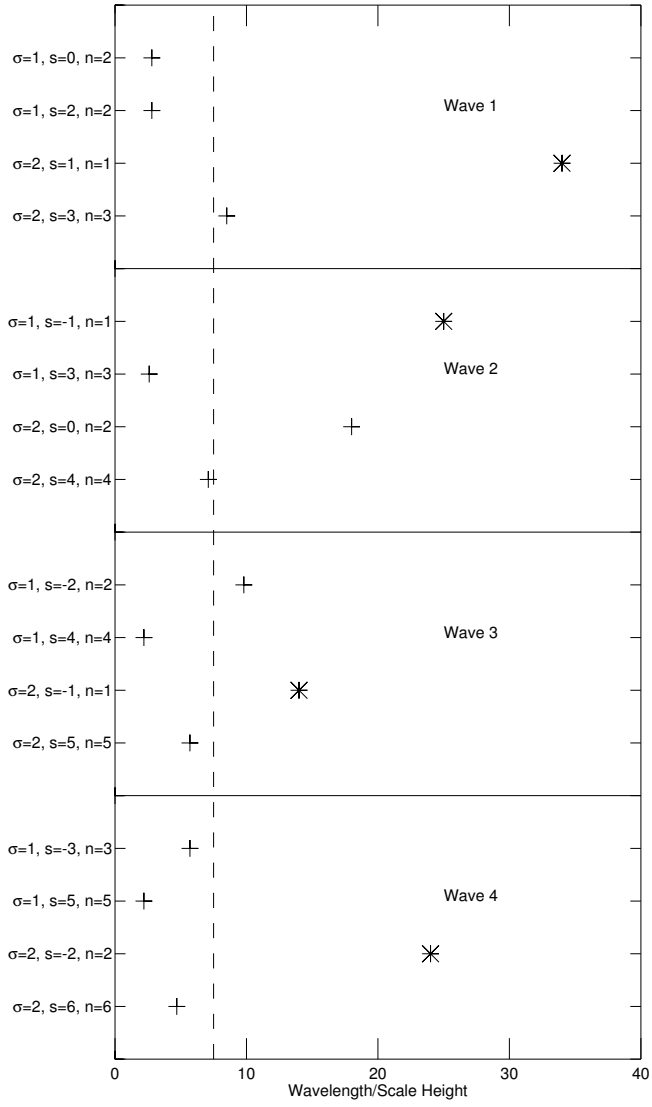

Figure 2.21: Vertical wavelengths of the 16 σ, s, n Hough modes that satisfy the excitation criteria. Travelling waves are marked with a cross and evanescent waves are marked with an asterisk. The dashed line represents the propagation criterion — Hough modes with vertical wavelengths greater than 7.5 scale heights can propagate to the upper atmosphere.

smallest vertical wavelength is 14 scale heights. Some of the travelling Hough modes have undergone 6 or more cycles before reaching this altitude, and they are damped to very low amplitudes in the upper atmosphere. Others have undergone less than a complete cycle before reaching this altitude, and they have not been damped to very low amplitudes. I assert that, of the Hough modes in Figure 2.21, the travelling Hough modes with vertical wavelengths greater than 7.5 scale heights and all the evanescent Hough modes can propagate to the upper atmosphere. Travelling Hough modes with shorter vertical wavelengths are damped to insignificance. This propagation criterion corresponds to travelling waves undergoing no more than two complete cycles before reaching 130 km altitude. This propagation criterion suggests that only the σ, s, n Hough modes listed in Table 2.4 are plausible causes of the zonal structure. In cases where more than one Hough mode could be causing a given zonal density harmonic, both could be operating simultaneously. The relatively rapid decrease in normalized amplitude of the wave-1 harmonic with altitude, discussed in Section 2.5.3, suggests its Hough mode has a shorter vertical wavelength than those causing the other zonal harmonics. This favours the $\sigma = 2, s = 3, n = 3$ Hough mode over the $\sigma = 2, s = 1, n = 1$ Hough mode in Table 2.4.

I do not consider the effects of winds on these Hough modes. Vertical propagation up from the lower atmosphere is affected by the zonal mean winds because these winds Doppler-shift the frequency of the Hough mode. A low frequency, or high period, means a longer time spent propagating through the dissipative regions and more dissipation. Dissipation increases when the tide propagates in the same direction as the zonal mean wind (Forbes et al., 2001). The accelerometer data are measured above eastward zonal winds in the northern hemisphere at the beginning of Phase 2 of aerobraking, then above westward zonal winds around the equator, and finally above eastward winds in the southern hemisphere at the end of Phase 2 of aerobraking (Leovy, 1982; Haberle et al., 1993; Forbes et al., 2001). The broad boundaries of these regions are marked by latitudes where there are eastward zonal wind at one altitude and westward zonal winds at another. This complicated situation is best suited to analysis by detailed modelling work, which is not the aim

Hough Mode	Zonal wavenumber at fixed LST	Wavelength in Scale Heights
$\sigma = 2,\ s = 1,\ n = 1$	1	34 (Evanescent)
$\sigma = 2,\ s = 3,\ n = 3$	1	8.5
$\sigma = 1,\ s = -1,\ n = 1$ (DK1)	2	25 (Evanescent)
$\sigma = 2,\ s = 0,\ n = 2$	2	18
$\sigma = 1,\ s = -2,\ n = 2$ (DK2)	3	9.8
$\sigma = 2,\ s = -1,\ n = 1$	3	14 (Evanescent)
$\sigma = 2,\ s = -2,\ n = 2$	4	24 (Evanescent)

Table 2.4: Hough modes satisfying the excitation and propagation criteria.

of this chapter, so I merely state that the different Hough modes are damped to different degrees by the zonal winds, that this damping changes with latitude and season, and that this omission affects my results to some extent.

Observations at widely spaced LSTs can be used to reject some of the possible Hough modes in Table 2.4. Diurnal and semidiurnal Hough modes, if contributing to the zonal structure, cause different changes in the phase of harmonics in the zonal structure over intervals of half a sol.

Recall from Section 2.5.5 that the phase of the wave-1 zonal density harmonic changed by 90 degrees over an interval of half a sol. A diurnal Hough mode would cause the wave-1 phase to shift by 180 degrees over this time and a semidiurnal Hough mode would cause no phase change at all. The phase of the wave-2 zonal density harmonic changed by 90 degrees over an interval of half a sol. A diurnal Hough mode would cause the wave-2 phase to shift by 90 degrees over this time and a semidiurnal Hough mode would cause no phase change at all. The phase of the wave-3 zonal density harmonic did not change over an interval of half a sol. A diurnal Hough mode would cause the wave-3 phase to shift by 60 degrees over this time and a semidiurnal Hough mode would cause no phase change at all. The wave-4 zonal density harmonic is not statistically significant in the nightside wavefit. These observations rule out some of the possible modes listed in Table 2.4.

The results of Section 2.5.5 (Table 2.3) lead me to conclude that the wave-1 zonal density harmonic is not associated with one of the two possible Hough modes in Table 2.4, the wave-2 zonal density harmonic is attributable to the $\sigma = 1, s = -1, n = 1$ Hough mode (DK1), the wave-3 zonal density harmonic to the $\sigma = 2, s = -1, n = 1$ Hough mode, and the wave-4 zonal density harmonic, where present, to the $\sigma = 2, s = -2, n = 2$ Hough mode. The wave-1 zonal density harmonic shows a phase change of about 90°, midway between the 0° change of a semidiurnal harmonic and the 180° change of a diurnal harmonic, so it cannot be explained by this simplified model. These preliminary conclusions are independent of any previous modelling or observational work, have neglected the effects of winds,

and are re-examined at the end of Section 2.6.2.

The studies of Hough modes in Section 2.6.1 were performed using computer programs kindly provided by Jeff Forbes.

2.6.2 Other Tidal Observations and Theory

In this section I discuss previous modelling and observational work on tides in the martian atmosphere that is relevant to Section 2.6.1 and then re-examine that Section's preliminary conclusions in light of the additional information.

Bougher et al. (2001) identified the $\sigma = 2, s = -1$ tidal mode as the most likely cause of the wave-3 harmonic they observed in both neutral density data and electron density data at 64–67°N latitude and $L_S = 70°$.

Joshi et al. (2000) used the results of Hollingsworth and Barnes (1996) to reject the hypothesis of Keating et al. (1998) that stationary waves were responsible for the zonal structure observed during Phase 1 of aerobraking. They also suggested that the observed zonal structure could be due to diurnally varying tidal modes. Simulations at 80 km altitude gave reasonable agreement with the observed phasing of the peaks.

Forbes and Hagan (2000) investigated the $\sigma = 1, s = -1, n = 1$ Hough mode (DK1). For simulated seasons applicable to Phase 1 of aerobraking, they found that DK1 could generate wave-2 zonal structure in upper atmospheric density. These simulations predicted an increase in normalized wave-2 amplitude with increasing altitude up to 200 km at $L_S = 270°$, unlike the decrease observed between 130 km and 150 km at $L_S = 30$–$90°$ in Section 2.5.3, and essentially no phase change with increasing altitude. In later simulations applicable to the observations in Section 2.5.3, Forbes et al. (2001) predicted that the amplitude in temperature of DK1 should be constant with altitude between 120 km and 200 km. Since density at a given altitude is sensitive to the vertically integrated temperature below it, this

implies that the normalized wave-2 amplitude in the density should increase from 120 km to 200 km.

Wilson has performed a series of tidal simulations (Wilson and Hamilton, 1996; Wilson, 2000a; Wilson, 2002). Wilson and Hamilton (1996) found that the $\sigma = 1, s = -1, n = 1$ Hough mode (DK1) had twice its usual amplitude during $L_S = 60$–$150°$, a period which includes the end of Phase 2 of aerobraking. This may contribute to the noticeable increase in the normalized wave-2 amplitude south of 15°N latitude in Figure 2.12 which is coincident with the arrival of $L_S = 60°$, though simulations also show increasing amplitude to the south at fixed season (Wilson, 2000a). In a comparison of TES temperatures with GCM results using a vertically averaged temperature with a broad weighting centred on 25 km altitude, Wilson (2000a) found that stationary waves, but not tides, are too confined in latitude to cause planet-wide zonal structure, that diurnal tides made larger contributions than semi-diurnal tides, and that each diurnal period, eastward propagating tidal mode had a deep vertical and broad meridional structure consistent with being dominated by the first symmetric Hough mode.

In simulations at 120 km altitude, Wilson (2002) found that the wave-2 zonal structure in the upper atmosphere was predominantly due to the $\sigma = 1, s = -1, n = 1$ Hough mode (DK1), the wave-3 zonal structure was a combination of the $\sigma = 1, s = -2, n = 2$ Hough mode (DK2) and the $\sigma = 2, s = -1$ tidal mode, and that these two wavenumbers dominate. He found the wave-3 zonal structure dominated by the diurnal mode in the tropics and by the semidiurnal mode in the extra-tropics, though he cautioned that those results were sensitive to the (uncertain) details of damping in the model. The wave-3 zonal structure has been observed to be dominated by semidiurnal tidal modes in high latitude observations by Bougher et al. (2001) and my Section 2.5.5. The simulated semidiurnal mode has little phase shift with changing altitude, the diurnal mode has more. Wilson did not address the wave-1 and wave-4 components of zonal structure. The $\sigma = 1, s = -1, n = 1$ Hough mode (DK1) provides a consistent description of the Viking

surface pressure data, TES temperatures at 25 km, and the wave-2 zonal density structure at 130 km, and has also has been observed in IRIS data from Mariner 9 (Conrath, 1976; Wilson, 2002).

Banfield et al. (2000) analysed tidal signatures in TES retrievals of lower atmospheric temperatures up to an altitude of ~40 km and south of 30°S latitude at L_S = 180–390° from Phase 1 of aerobraking and the Science Phasing Orbits. They examined the eight σ, s tidal modes with a σ, s, n Hough mode shown in Figure 2.21 that could cause wave-1 or wave-2 zonal structure and found that the $\sigma = 1, s = -1$ tidal mode was largest, followed by the $\sigma = 1, s = 0$ tidal mode. The first of these two tidal modes is probably dominated by the $\sigma = 1, s = -1, n = 1$ Hough mode (DK1) discussed above. The second of these two tidal mode, which causes zonal wave-1 structure, was identified in simulations of temperatures centred on 25 km as the dominant mode in the zonal wave-1 structure by Wilson (2000a). All of the tidal amplitudes of Banfield et al. (2000) suggested increases northward of 30°S. Smith et al. (2001) presented TES data from the later mapping mission, but did not repeat the detailed analysis of Banfield et al. (2000) of the tidal modes. However, a mix of tidal modes is present in their data. Since I have found wave-3 to be a much greater contributor to the zonal structure in the upper atmosphere than wave-1, it would be interesting to repeat the work of Banfield et al. (2000) including wave-3 modes.

Banfield et al. (2003) have also analysed tidal signatures in TES retrievals from post-aerobraking data. Their Figure 11 is probably dominated by the $\sigma = 1, s = -1$ tidal mode and the $\sigma = 1, s = -1, n = 1$ Hough mode (DK1). It shows a relatively weak amplitude during the season corresponding to Phase 2 aerobraking. Like my Figure 2.14, it shows highest amplitudes at the equator and higher amplitudes in the southern hemisphere than in the northern hemisphere. The longitude of the maximum is ~40°E in their lower atmosphere data and ~80°E in my upper atmosphere data, suggesting phase changes with height. Their Figure 12 is probably dominated by the $\sigma = 1, s = -2$ tidal mode and the $\sigma = 1, s = -2, n = 2$

Hough mode (DK2). This is restricted to the tropics in their observations and cannot be responsible for the strong wave-3 harmonic which I observe in the extra-tropics (my Figure 2.15). In Banfield et al. (2003), the maximum amplitude of the $\sigma = 2, s = -1$ tidal mode is no more than half that of DK2. However, since it is not restricted to the tropics, it could be the strongest contributor to the wave-3 zonal harmonic in the upper atmosphere, which would be consistent with my observations of a semidiurnal tidal mode for this harmonic in the southern polar regions.

Unambiguous identification of a particular Hough mode in the martian atmosphere requires many observations. The zonal wavenumber and period of the disturbance must be measured using observations at varied longitudes and LSTs. The meridional profile of the disturbance must be measured using observations at varied latitudes. The vertical profile of the disturbance must be measured using observations at varied altitudes. Observations of the background state of the atmosphere must be used in conjunction with modelling work beyond the classical tidal theory to predict the behaviour of candidate Hough modes as they are generated at the surface and propagate upwards through the spatially and temporally varying lower atmosphere. I am not able to satisfy all these requirements in this chapter. My identifications of certain Hough modes in this chapter are based primarily upon the observed density variations with longitude at fixed LST at many latitudes, the observed density variations with longitude near the South Pole at two LSTs half a sol apart, and classical tidal theory. These restrictions should be understood before the conclusions of this chapter are accepted by the reader. I discuss ways to test my conclusions in Section 2.9.

In summary, my conclusion that the wave-2 zonal structure is attributable to the $\sigma = 1, s = -1, n = 1$ Hough mode (DK1) is consistent with much observational and theoretical work. My conclusion that the wave-3 zonal structure is attributable to the $\sigma = 2, s = -1, n = 1$ Hough mode is consistent with theoretical work and observations at high latitudes, but theoretical work suggests that the $\sigma = 1, s = -2, n = 2$ Hough mode (DK2), which I rejected based on the observed

phase change at high latitudes, may be important at low to mid-latitudes. Observational and theoretical work in the lower atmosphere predicts that the $\sigma = 1, s = 0$ tidal mode dominates the zonal wave-1 structure, but I rejected it as a major influence in the upper atmosphere due to its short vertical wavelength. There has been little work relevant to the wave-4 zonal structure. I make one modification to my preliminary conclusions from Section 2.6.1. Previously rejected, the $\sigma = 1, s = -2, n = 2$ Hough mode (DK2) may make a significant contribution to the wave-3 zonal structure in the tropics.

2.6.3 Effects of the Surface on Zonal Structure

The zonal structure in the upper atmosphere must be caused by a zonal asymmetry in the lower boundary conditions of the atmosphere interacting with solar heating to excite a non-migrating tide. In this section I investigate which zonal asymmetry might have the strongest influence on the zonal structure.

Dust loading is variable on relatively short timescales, so it is unlikely to be responsible for the long-lasting, stable zonal structure. Information on the spatial distribution of dust is available from archived TES results, but recent publications have focused on the dust distribution during dust storms and not during the relatively calm period of Phase 2 of aerobraking (Smith et al., 2000; Smith et al., 2001).

Continuing from Section 2.6.1, it seems reasonable that the meridional profile of the zonal asymmetry that, in conjunction with solar heating, can excite a given Hough mode must overlap significantly with the meridional profile of solar heating (peaked in the tropics, equatorially symmetric, and without any minima close to the equator) for that Hough mode to be efficiently excited. Using Mars Consortium data kindly supplied to me by Jim Murphy and MOLA topography, I performed harmonic decompositions of topography, thermal inertia, and albedo as a function of longitude at different latitudes (Smith et al., 2001b). As shown

in Figure 2.22, the wave-1 component of topography is low near the equator and highest in the extra-tropics. The wave-2 component of topography has high amplitudes throughout the tropics, is greatest at the equator, and decreases into the extra-tropics. Except for a narrow region of low amplitude at 30°S, it is reasonably symmetric about the equator. The wave-3 component has high amplitude at the equator, is quite constant throughout the tropics, and decreases rapidly poleward of 60°. The wave-4 component of topography is low near the equator and highest in the extra-tropics. All amplitudes are below 0.6 km in smooth terrain poleward of 60°. The wave-2 and wave-3 components of topography satisfy the overlap criteria, but none of the components of albedo or thermal inertia do. As discussed in Section 2.6.1, both these components of topography can generate Hough modes with the ability to propagate into the upper atmosphere and appear as wave-2 and wave-3 zonal structure. This is consistent with the observation in Section 2.5.4 that these harmonics are the strongest. Figure 2.23 shows a contour map of martian topography so that the harmonic breakdown in Figure 2.22 can be related to actual topographic features.

It has already been shown that topography, the range of which exceeds an atmospheric scale height, is the main cause of the $\sigma = 1, s = -1, n = 1$ Hough mode (DK1) (Wilson and Hamilton, 1996; Wilson, 2002). This justification for the dominance of wave-2 and wave-3 harmonics in the zonal structure is intended to offer some physical insight as a complement to the rigorous results of more complete models. It could be tested by repeating the work of Wilson and Hamilton (1996) on the $\sigma = 1, s = -1, n = 1$ Hough mode (DK1) on the other Hough modes that are possible contributors to the zonal structure.

2.7 Mars Odyssey and Mars Reconnaissance Orbiter

Aerobraking for Mars Odyssey began in late October, 2001, and was successfully concluded in mid-January, 2002. Approximately 330 orbits of data are currently

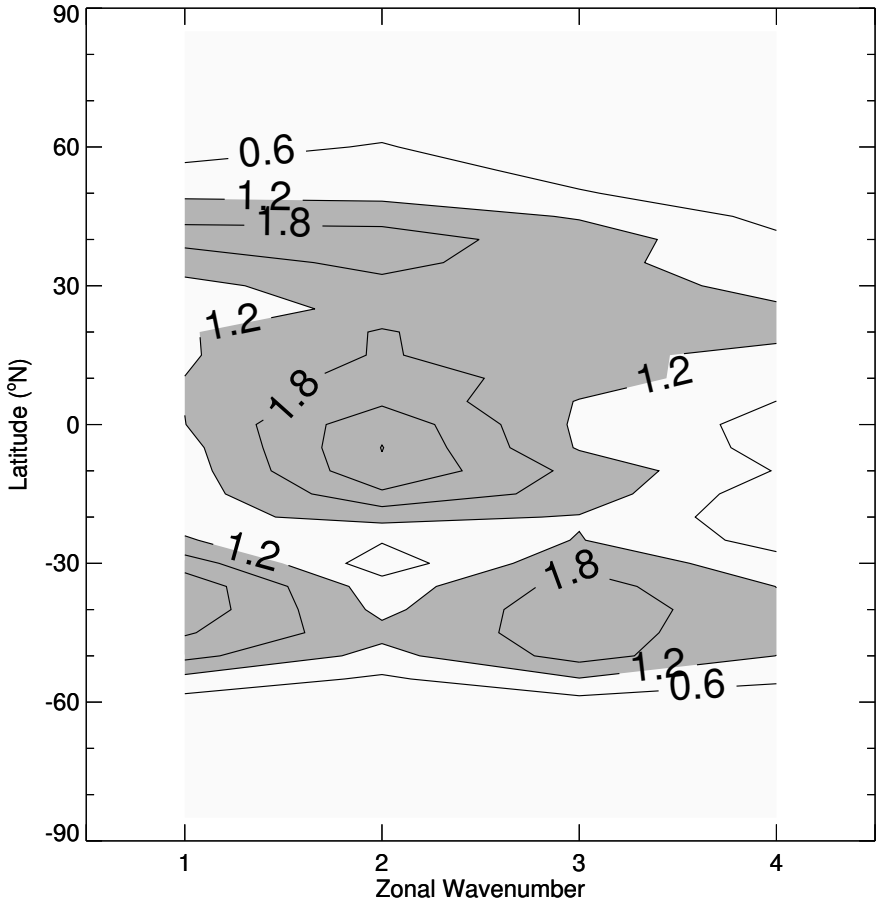

Figure 2.22: Amplitudes, in km, of the various zonal harmonics in martian topography as a function of latitude. Contour intervals are 0.6 km and values greater than 1.2 km are shaded.

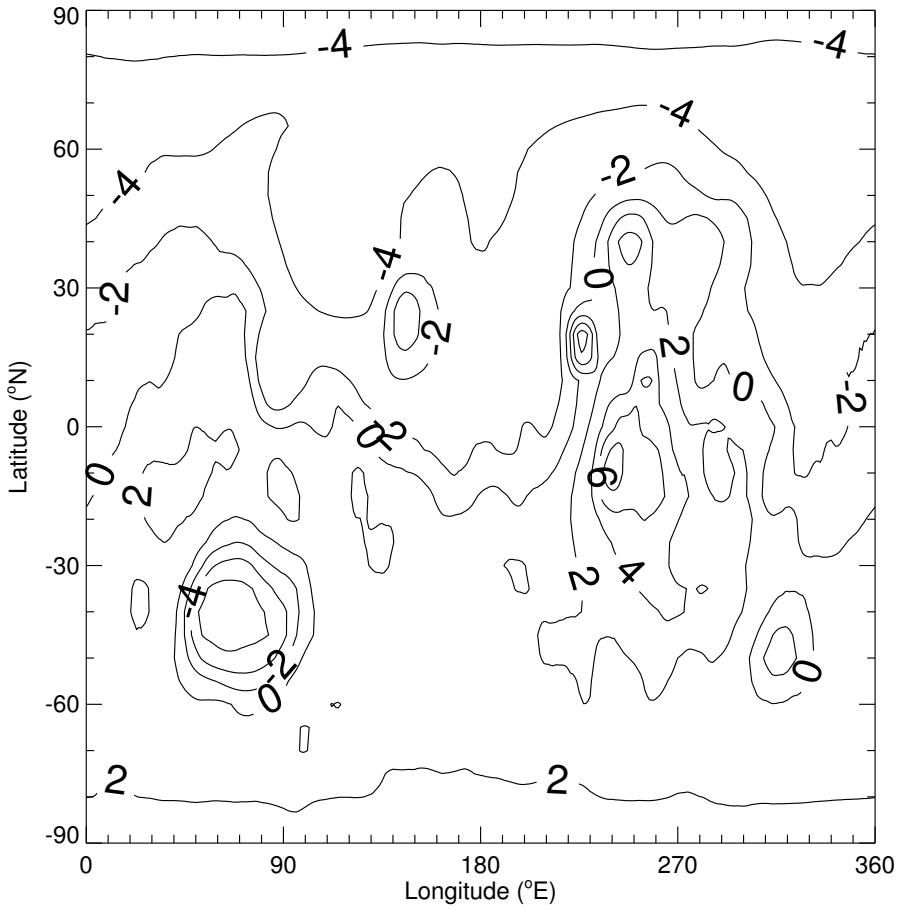

Figure 2.23: Low-resolution contour map of martian topography from MOLA. Contour intervals are 2 km.

being processed and analysed by Keating and colleagues. Results will be published in due course. At the beginning of aerobraking, periapsis occurred at $L_S = 260°$, latitude = 70°N, LST = 18 hours, then precessed northward through midnight LST and across the pole, and continued southward until the end of aerobraking at $L_S = 310°$, latitude = 20°N, LST = 03 hours. Odyssey's aerobraking occurred at a different time in the 11-year solar cycle from that of MGS, and shortly after one of the largest global dust storms ever recorded.

The next anticipated aerobraking dataset is that of the Mars Reconnaissance Orbiter (MRO), scheduled for launch in 2005. The accelerometer instrument on this spacecraft has been upgraded in status from an engineering instrument to a facility science instrument and its high sensitivity promises useful data at altitudes near the exobase during both the aerobraking and the main phases of the mission. The predictions in this chapter for sol-to-sol variability are useful to JPL in their ongoing preparation of MRO's nominal aerobraking plan.

2.8 Future Work

In this section, I discuss opportunities to further develop my work on tides and zonal structure in the martian upper atmosphere. They include searches for temporal effects, study of density scale heights at the same fixed altitudes as this density work, analysis of the individual density profiles and derivation of pressure, temperature, and wind results, examination of Phase 1 data, incorporation of data from other MGS instruments, extension to Mars Odyssey data, and comparisons to useful models.

Upper atmospheric densities are not perfectly described by the fitted zonal structure. Do deviations from the fitted zonal structure have any temporal structure that would suggest the effects of long period waves, such as may be caused by the 28 day solar rotation period, or short term phenomena, such as solar flares? Is high sol-to-sol variability correlated with known periods of high solar activity?

The MGS inbound and outbound data can be carefully compared to identify how stable the zonal structure is on weekly timescales. For example, is the amplitude of the wave-2 harmonic at a given latitude always smaller on inbound than outbound? Is it always smaller relative to the wave-3 harmonic on inbound rather than outbound? These detailed questions have not been addressed in this chapter.

The PDS dataset used throughout this chapter gives density scale heights at fixed altitudes and the altitudes of the 1.26 nbar pressure level for each aerobraking pass, in addition to densities (Keating et al., 2001b). These could be examined for zonal structure or other interesting behaviours.

The individual density profiles from each aerobraking pass contain much more information than the handful of densities extracted at several altitude levels (Keating et al., 2001a). As Chapters 3 and 4 discuss, I am in the early stages of using the assumptions of hydrostatic equilibrium and a uniform zonal wind to derive corresponding pressure and temperature profiles and a zonal wind estimate for each density profile. There have been no previous measurements of winds in the martian upper atmosphere. These new pressure and temperature profiles can be examined for differences between their zonal structure and that of the density data. The accelerometer temperature profiles can be examined for migrating tidal signatures, as have previously been seen in temperature profiles from landers, or gravity waves (Magalhães et al., 1999; Seiff and Kirk, 1977a). The density profiles contain occasional sudden changes in density/acceleration that are still unexplained (Tolson et al., 1999). Densities at any fixed altitude can be extracted from the density profiles and used to study the zonal structure at altitudes as low as about 105 km. Combined with a careful study of the 160 km data, paying due attention to the uncertainties, this increased altitude range may reveal phase shifts in the zonal structure with changing altitude.

The Phase 1 data cover latitudes similar to those at the start of Phase 2 at a different season. They could be studied to examine seasonal changes in the zonal

structure. They also include the upper atmosphere's response to the rise and fall of a regional dust storm, so changes in the upper atmosphere could be compared to changes in winds and vertical temperature structure in the lower atmosphere. The sol-to-sol variability can also be studied at this different season, because Phase 1 contains the 1:1 and 2:1 resonances.

Data from the Mars Horizon Sensor Assembly at several different LSTs will help identify the tidal modes present in the atmosphere (Martin and Murphy, 2001; Murphy et al., 2001). Since Bougher et al. (2001) have used Radio Science observations to show that zonal structure exists in electron densities that appears to mimic that in the neutral densities, other electron density observations from this and possibly other missions can be examined for zonal structure. This permits analysis of changes in the zonal structure with season and LST, for example.

The Mars Odyssey data, when publicly released, will complement the MGS data by covering different latitudes, LSTs, and season. All my analysis techniques, applied here to MGS data, can be readily applied to Odyssey data.

Current surface-bounded GCMs barely reach the lowest aerobraking altitudes (Angelats i Coll et al., 2001; Wilson, 2002). When they are able to span the full altitude range of aerobraking data, or when joint lower atmosphere-upper atmosphere models are coupled closely enough to allow tidal propagation, comparing the accelerometer data with model simulations will be a fruitful avenue for many research paths (Bougher et al., 1999).

In summary, there are many other investigations that can increase our understanding of tides and zonal structure in the martian upper atmosphere in the near future.

2.9 Conclusions

Sol-to-sol variability, or weather, in the martian upper atmosphere is not well modelled by current climate models. As martian climate models develop into weather models with the goal of understanding and interpreting the results of current and anticipated long-term, global-scale, atmospheric monitoring from orbiting instruments with high spatial and temporal resolutions, this variability with short spatial and temporal scales at high altitudes will provide a challenging test of their abilities. This variability is also significant for the design of future aerobraking missions.

For the seasons and latitudes discussed here, the sol-to-sol variability at fixed longitude, altitude, latitude, LST, and season is smaller than the longitudinal variability at fixed altitude, latitude, LST, and season. This repeatable variation with longitude, or zonal structure, can cause densities to change by a factor of two or more over less than 90° of longitude. The zonal structure must be due to thermal tides generated at or near the planet's surface. It is remarkable that surface effects are so significant at altitudes of 150 km.

I have used the changes in the zonal structure with altitude, latitude, and LST, together with a simple application of classical tidal theory, to identify the tidal modes that have the strongest contributions to the zonal structure. The week-to-week stability of the zonal structure and its similar behaviour at all latitudes require a planetary-scale, not localized, phenomenon. The $\sigma = 1, s = -1, n = 1$ (wave-2, DK1) and $\sigma = 2, s = -1, n = 1$ (wave-3) Hough modes have been identified as major contributors to the zonal structure and this is supported by previous theoretical work. The $\sigma = 1, s = -2, n = 2$ (wave-3, DK2) Hough mode is predicted to be present. The wave-4 component of the zonal structure is attributed to the $\sigma = 2, s = -2, n = 2$ Hough mode and the cause of the weak wave-1 component is uncertain. I have presented a simple justification, based on the meridional profiles of solar heating and of various harmonic components of topography, thermal inertia, and albedo, for why the wave-2 and wave-3 components dominate the zonal structure

and suggested that both are controlled by topography.

I believe that my conclusions are robust, although, as discussed in Section 2.6.2, these Hough modes have been identified indirectly. The main ways in which they might be tested are (a) observations of the zonal wavenumbers and periods of any zonal structure in the middle atmosphere which would test my conclusion that certain Hough modes are propagating through the middle atmosphere, (b) upper atmospheric observations at more varied longitudes and LSTs, which, by identifying the zonal wavenumbers and periods of the zonal structure, would test my identification of certain Hough modes in the upper atmosphere, and (c) detailed modelling work, which would test my simplified ideas about vertical propagation of Hough modes. For consistency, these new observations would be most useful if they occurred at the same L_S as the MGS accelerometer observations.

At the surface of the Earth, atmospheric tides are often small-scale fluctuations masked by the effects of weather and only detectable in long duration records. At higher altitudes, they are more prominent. On Mars, whose atmosphere has a greater diurnal variation in solar heating per unit mass than Earth's, tidal effects are greater. They are a major feature in the long-term pressure measurements at the two Viking landing sites and were predicted by the very first martian climate model (Leovy and Mintz, 1969; Zurek et al., 1992). Tides have long been recognized as a basic feature of the dynamics of the martian lower atmosphere; this work, and others, demonstrates that they are important in the upper atmosphere as well. As such, upper atmosphere models which do not have dynamic connections to lower atmosphere models will be unable to reproduce observations or make accurate predictions.

The strength of a tidal mode in the martian upper atmosphere depends on the winds and temperatures in the lower atmosphere. If surface-to-thermosphere models can reliably reproduce the upper atmosphere observations, then only those lower atmosphere conditions which correspond to the observed behaviour in the upper atmosphere are permissible. This offers a way to constrain the behaviour of

the lower atmosphere using only observations from the upper atmosphere.

Accelerometers are the only scientific instruments that will fly again and again into Mars orbit during the next decade. As such, they offer a unique way to study the behaviour of the difficult-to-study upper atmosphere over inter-annual periods and the 11-year solar cycle. Their observations are difficult to compare to most current martian climate models because of their high altitude, and this partially explains why so few recent publications have discussed accelerometer data, but they still have value. Accelerometer datasets will be invaluable in the future when, inevitably, models reach such altitudes, and every opportunity should be taken now to collect and preserve such datasets.